

Geochemistry, Geophysics, Geosystems



RESEARCH ARTICLE

10.1029/2023GC010993

Key Points:

- We compare new hematite (U-Th)/He dates with previously published paleomagnetic data from the same exposure of crystalline basement rock
- Hematite (U-Th)/He dates are younger than the inferred timing of magnetization and imply partial He loss since magnetization acquisition
- (U-Th)/He dates may not relate to remanence acquisition because of differences in sampling requirements and temperature sensitivity

Supporting Information:

Supporting Information may be found in the online version of this article.

Correspondence to:

J. L. Jensen, jljensen@usu.edu

Citation:

Jensen, J. L., Ault, A. K., & Geissman, J. W. (2023). Evaluating the compatibility of hematite (U-Th)/He data and hematite-carried secondary magnetizations: An example from the Colorado Front Range. *Geochemistry, Geophysics, Geosystems*, 24, e2023GC010993. https://doi.org/10.1029/2023GC010993

Received 7 APR 2023 Accepted 17 AUG 2023

Author Contributions:

Conceptualization: Alexis K. Ault, John W. Geissman
Formal analysis: Jordan L. Jensen,
Alexis K. Ault, John W. Geissman
Funding acquisition: Alexis K. Ault
Investigation: Jordan L. Jensen, Alexis
K. Ault, John W. Geissman
Supervision: Alexis K. Ault
Visualization: Jordan L. Jensen, John W. Geissman

© 2023 The Authors. Geochemistry, Geophysics, Geosystems published by Wiley Periodicals LLC on behalf of American Geophysical Union. This is an open access article under the terms of the Creative Commons Attribution License, which permits use, distribution and reproduction in any medium, provided the original work is properly cited.

Evaluating the Compatibility of Hematite (U-Th)/He Data and Hematite-Carried Secondary Magnetizations: An Example From the Colorado Front Range

Jordan L. Jensen¹, Alexis K. Ault¹, and John W. Geissman^{2,3}

¹Department of Geosciences, Utah State University, Logan, UT, USA, ²Department of Geosciences, University of Texas at Dallas, Richardson, TX, USA, ³Department of Earth and Planetary Sciences, University of New Mexico, Albuquerque, NM, USA

Abstract Ancient magnetization(s), often recorded by hematite (Fe₂O₂), provide key paleomagnetic constraints on plate interactions through time. Primary remanent magnetizations may be modified or overprinted by secondary processes that complicate interpretations of paleomagnetic data. Hematite (U-Th)/He (hematite He) dating has the potential to resolve when secondary magnetizations were acquired. Here, we compare hematite He data and paleomagnetic results in Paleoproterozoic crystalline rocks, meters below a major nonconformity in the Colorado Front Range, USA. Prior work and new rock magnetic data indicate that pervasive hematite alteration records a secondary chemical remanent magnetization (CRM) during the Permo-Carboniferous Reverse Superchron, coincident with the Ancestral Rocky Mountain orogeny. We target minor hematite-coated faults cutting basement for (U-Th)/He analyses because they are of sufficient hematite purity to yield geologically meaningful dates. Two samples yield overlapping and scattered individual hematite He dates ranging from \sim 138 to 27 Ma (n = 33), significantly younger than the age of the late Paleozoic CRM. Scanning electron microscopy, electron probe microanalysis, and Raman spectroscopy indicate that aliquots have variable grain size distributions and fluorocarbonate impurities. Thermal history models support hematite on fault surfaces mineralized coeval with CRM acquisition during the late Paleozoic, and hematite He data scatter reflects variable He loss during Mesozoic burial owing to differences in grain size distribution from fault slip comminution and in chemistry among aliquots. Our results underscore the differences in temperature sensitivity and sampling requirements between paleomagnetic and hematite He investigations and illustrate that hematite He dates will usually be younger than preserved remanent magnetizations.

Plain Language Summary Minerals such as hematite are capable of recording the direction of the Earth's magnetic field during formation and this paleomagnetic information helps geoscientists estimate the age of rocks and the past motions of tectonic plates. During geologic events like mountain-building, primary paleomagnetic signatures in rocks may be modified or replaced by new, secondary paleomagnetic recordings. Such secondary magnetizations can be challenging to interpret, especially if the age of these magnetizations is unknown. (U-Th)/He analysis, a form of radiometric dating, may aid paleomagnetic studies by revealing the age of minerals that carry secondary magnetizations. In this study, we compare hematite (U-Th)/He data and a secondary magnetization carried by hematite from Colorado's Front Range and find that (U-Th)/He dates are scattered and considerably younger than the reported age of the secondary magnetization. We interpret the variability of hematite (U-Th)/He dates to reflect differences between aliquots relating to crystal size and the presence of non-hematite minerals. Our results suggest that the (U-Th)/He system was partially to fully reset by a more recent phase of burial and associated reheating that was not hot enough to fully reset the paleomagnetic system. We conclude that (U-Th)/He and paleomagnetic investigations in hematite may not record the same geologic events.

1. Introduction

Paleomagnetic data provide estimates of the timing and relative location of rock formation or alteration (e.g., Butler, 1992; Torsvik, 2005). These data serve as principal constraints in plate motion reconstructions and anchor our chronicling of plate interactions through time, including through the supercontinent cycle (Domeier et al., 2012; Gordon et al., 1984; Meert, 2001; Zhang et al., 2012). A central objective of paleomagnetic investigation is determining the origin and age of natural remanent magnetizations (NRM) in rocks containing

JENSEN ET AL. 1 of 22

15252027, 2023, 9, Downloaded from https

Writing – original draft: Jordan L. Jensen Writing – review & editing: Jordan L. Jensen, Alexis K. Ault, John W. Geissman ferrimagnetic/canted antiferromagnetic minerals (e.g., Fe oxides like magnetite and hematite). NRMs can be represented by one or multiple components that are primary (acquired during rock formation) or secondary (acquired after rock formation) in nature. Distinguishing between primary and secondary components can be challenging because many geologic processes including secondary mineralization and heating due to regional burial can alter or overprint NRMs, long after the initial formation of rock units (e.g., Elmore et al., 2012; Huang et al., 2023; Larson et al., 1982; Pullaiah et al., 1975; Roy & Park, 1972). Failing to recognize altered primary or secondary components of NRMs can result in erroneous plate reconstructions and paleomagnetic-based chronologies (e.g., Huang et al., 2017, 2023). Geochronologic data from the same Fe oxides that carry NRMs, independent of the paleomagnetic system, could thus prove useful in identifying and assigning temporal constraints to primary and secondary components of NRMs and ultimately lead to more refined interpretations of paleomagnetic data sets.

(U-Th)/He thermochronometry of hematite (hematite He), a common Fe oxide, has the potential to reveal the timing of magnetic overprinting in rocks, considering that secondary components of NRMs are commonly associated with the formation of secondary hematite. The (U-Th)/He method was developed as one of the first radiometric dating techniques in the early 20th century, but fell out of favor when it was recognized that diffusive loss of radiogenic He can be substantial at low to moderate temperatures (Strutt, 1910). Renewed interest in the hematite He method has been facilitated by a more robust understanding of He diffusivity in this phase (Bähr et al., 1994; Evenson et al., 2014; Farley, 2018; Farley & Flowers, 2012; Wernicke & Lippolt, 1993). Under certain conditions, hematite can retain most or all of its radiogenic He over geologic timescales. Hematite He thermochronometry has been used to document continental weathering reactions (Monteiro et al., 2022), fault slip (Ault et al., 2015; DiMonte et al., 2022; McDermott et al., 2017; Moser et al., 2017), and hydrothermal mineralization (Jensen et al., 2018; Wu et al., 2018).

We evaluate the potential of combined paleomagnetic and (U-Th)/He studies in hematite. Specifically, we test whether the hematite He system can corroborate the age of a well-developed, ancient yet secondary chemical remanent magnetization (CRM) carried by hematite in Paleoproterozoic crystalline basement rocks exposed below regional nonconformity in central Colorado, USA (Geissman & Harlan, 2002). Here, we report new rock magnetic data that confirm hematite is the magnetic carrier of the CRM, supporting the interpretations of Geissman and Harlan (2002). The secondary magnetization was acquired in the late Paleozoic and is observed in multiple basement assemblages of different ages found throughout the Southern Rocky Mountains (Geissman & Harlan, 2002). This further bolsters the late Paleozoic age constraint of the magnetization characteristic of the rocks at our study locale and makes it an ideal benchmark to compare with our hematite He dates.

We target hematite from fault surfaces that cut crystalline rock for hematite He analyses because, in stereoscope, they are of sufficient thickness and hematite purity to yield geologically meaningful dates. Field observations, petrographic, scanning electron microscopy (SEM), electron probe microanalysis (EPMA), and Raman spectroscopy data are used to evaluate the sources of intrasample scatter in hematite He dates. We use simple thermal history models to assess if hematite could have precipitated in the late Paleozoic, consistent with the paleomagnetic data, and to consider how the evolving grain size distribution controls post-mineralization He loss. Finally, we discuss the compatibility between paleomagnetic and hematite He data sets and show that the observed disparity between the timing and processes that these systems record can be reconciled by considering differences in sampling requirements and in their thermal sensitivity as a function of domain structure.

2. Background

2.1. Geologic Framework and Evidence for Late Paleozoic Hematite Alteration

The Southern Rocky Mountains in the western United States is a physiographic province with a mean elevation >2,500 m above sea level and hosts the highest peaks of the entire Rocky Mountains. The area experienced extensive thick-skinned, high-angle reverse faulting during the Late Cretaceous-Eocene Laramide orogeny (~70–45 Ma), although some of the current high elevation is possibly attributed to post-Laramide epeirogenic uplift (Abbott et al., 2022; Cather et al., 2012; Eaton, 2008). The high peaks of the Southern Rockies have since been denuded by fluvial processes and alpine glaciation during Pleistocene glacial periods (e.g., Benson et al., 2005). Many of the subranges within the Southern Rockies are cored by ~1.8–1.7, ~1.4, and ~1.1 Ga crystalline basement rocks (Whitmeyer & Karlstrom, 2007, and references therein; Figure 1a). In the Front Range of

JENSEN ET AL. 2 of 22

5252027, 2023, 9, Downloaded from https://agupubs.onlinelibrary.wiley.com/doi/10.1029/2023GC010993, Wiley Online Library on [16/09/2023]. See the Terms

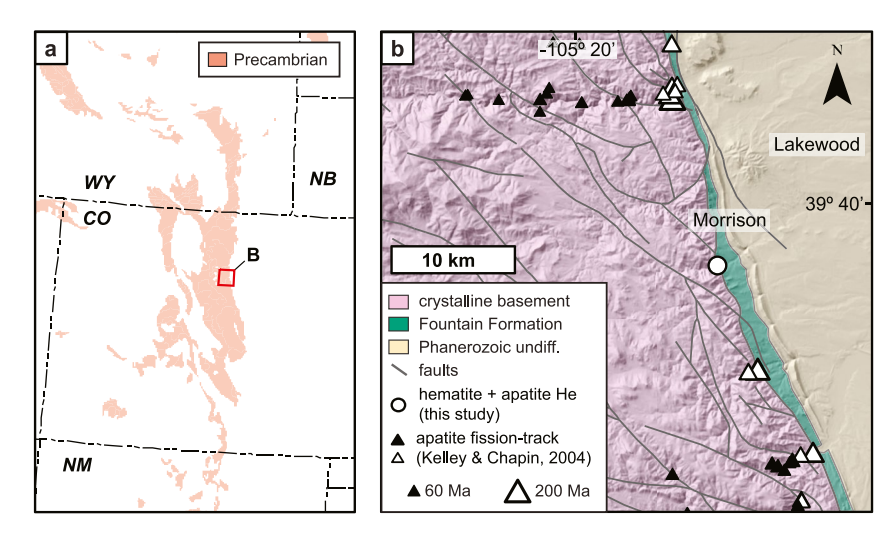


Figure 1. Geologic and sample location maps. (a) Simplified geologic map modified after Reed et al. (2004) showing locations of Precambrian exposures in Colorado and surrounding states. (b) Topographic hillshade overlain by a simplified geologic map modified after Tweto (1979) that subdivides geologic units into Precambrian crystalline basement, the Pennsylvanian Fountain Formation, and undifferentiated (undiff.) Phanerozoic rocks. Our sampling location (white circle) lies on the boundary between crystalline basement and the Fountain Formation, which are in nonconformable contact at this locality. Apatite fission-track (AFT) data of Kelley and Chapin (2004) are shown for reference, with triangle size scaling with AFT date between 60 and 200 Ma (black triangles <100 Ma and white triangles >100 Ma).

Colorado, nonconformable contacts between Proterozoic basement and Cambrian through Pennsylvanian sedimentary rocks are exposed on the eastern flank of basement-cored uplifts (Figure 1) and indicate that basement rocks were at or near the paleosurface prior to deposition of the sedimentary cover (Tweto, 1979). Thermochronometric data from nearby basement transects and basement-hosted sandstone injectites suggest that basement exposure to the near surface significantly predates the depositional age of overlying sediments (Flowers et al., 2020; Havranek & Flowers, 2022; Jensen et al., 2018; Ricketts et al., 2021), implying the nonconformable contacts represent composite erosional surfaces that initially developed in the Neoproterozoic.

Our study area, approximately 3 km south of Morrison, CO (USA), is on the eastern margin of the central Front Range (Figure 1) and displays a crystalline basement-sedimentary contact inferred to be a Pennsylvanian erosional surface that culminated during the late Paleozoic Ancestral Rocky Mountain orogeny (ARMO; Kluth & Coney, 1981; Leary et al., 2017). Lower Paleozoic shallow marine sandstone and carbonate rocks preserved elsewhere in the Front Range were deposited and later eroded in the region of our study locality during ARMO unroofing (Kellogg et al., 2004; Pearson & Johnson, 1980). Regional continuity of lower Paleozoic passive margin strata is supported by clasts of lower Paleozoic rocks within the Pennsylvanian Fountain Formation (Sweet et al., 2015), which is the sedimentary sequence deposited directly on the basement at our study location (Scott, 1972). The Fountain Formation records deposition of arkosic detritus shed from ARMO highlands eastward into adjacent basins and forms the base of a ~3–4 km-thick sequence of upper Paleozoic to lower Cenozoic basin fill composed chiefly of sandstones, siltstones, and mudstones (Kellogg et al., 2008; Scott, 1972). The basal section of the Fountain Formation has extensive Fe oxide alteration and staining with abundant authigenic hematite that extends into the underlying basement rocks, implying that the nonconformity acted as a conduit for Fe-rich paleofluids sometime after the deposition of the Fountain Formation.

The paleomagnetism and magnetic properties of rocks delineating the Proterozoic-Pennsylvanian nonconformity at our study site, as well as other nonconformities in the Southern Rocky Mountains, were characterized by Geissman and Harlan (2002). Basement samples of different Proterozoic age from several localities immediately below nonconformities exposed in Colorado, New Mexico, and Wyoming all yield magnetizations with an S-SE declination and a shallow, commonly negative, inclination. The authors interpret the observed magnetization as a secondary, yet ancient CRM carried by hematite. This CRM was acquired during the Permo-Carboniferous Reverse Polarity Superchron (PCRS; Irving & Parry, 1963; Opdyke, 1995), soon after deposition of the overlying Fountain Formation. The late Paleozoic CRM is interpreted to have resulted from alteration in association with <200°C Fe-bearing basinal brines migrating along the nonconformity during the waning stages of the ARMO

JENSEN ET AL. 3 of 22

15252027, 2023, 9, Downloaded from https:

//agupubs.onlinelibrary.wiley.com/doi/10.1029/2023GC010993,

Wiley Online Library on [16/09/2023]. See the Terms

(~early Permian; Geissman & Harlan, 2002). Similar late Paleozoic CRMs have been documented in crystalline and sedimentary rocks within the Southern Rocky Mountains as well as globally (Creer, 1968; Preeden et al., 2009; Van der Voo & French, 1977; Wawrzyniec et al., 2007).

During the Mesozoic, following the ARMO, sedimentary environments transitioned from mostly terrestrial settings to nearshore and marine environments formed in response to the inundation of the Western Interior Seaway, before returning to dominantly terrestrial depositional environments in the latest Cretaceous and Paleogene (Elder & Kirkland, 1994). The thickest accumulations of Mesozoic strata were deposited during the Cretaceous marine phase and mark maximum burial prior to Laramide exhumation (Weimer & Sonnenberg, 1996). The marine sequence includes the \sim 70 Ma Pierre Shale that is \sim 2 km thick in our study area (Scott, 1972) and that thickens to the northwest (Tourtelot, 1962). The onset of Laramide crustal shortening coincides with the regression of the Western Interior Seaway and the recurrence of nearshore, coastal, and fluvial sedimentary regimes (Kellogg et al., 2004).

Burial prior to Laramide exhumation was not sufficient to completely overprint the PCRS CRM. Geissman and Harlan (2002) reported three examples of thermal demagnetization results. In Figure S1 in Supporting Information S1, we show additional examples of the response to progressive thermal demagnetization of specimens from the MR1 locality of Geissman and Harlan (2002). These data further enforce the observation that these rocks carry a well-defined SSE-declination, moderate positive inclination (in geographic coordinates) magnetization, interpreted to be a CRM of late Paleozoic vintage. Some of the samples carrying the CRM display a minor magnetization component that is variable in direction and that unblocks between ~400 and 500°C (e.g., sample 48Aa in Figure S1 in Supporting Information S1).

Regional and local low-temperature thermochronometry data from Paleoproterozoic basement rocks bracket the timing of Laramide contraction and associated unroofing of basement-cored blocks to ~70-45 Ma (Abbey et al., 2018; Bryant & Naeser, 1980; Havranek & Flowers, 2022; Johnson et al., 2017; Kelley & Chapin, 2004; Naeser et al., 2002). For example, in the Front Range, apatite fission-track (AFT) thermochronometry yields "pre-Laramide" dates (>100 Ma) at the eastern range margin near our study area and "Laramide" dates (80-53 Ma) within the range core, permitting identification of the base of the Laramide-age AFT partial annealing zone (PAZ; corresponds to a ~110°C fossil isotherm) (Kelley & Chapin, 2004). Kelley and Chapin (2004) interpret the preservation of older, pre-Laramide AFT dates from the eastern margin to indicate lower peak burial temperatures compared to the range core, coupled with an increased magnitude of exhumation. Additional factors contributing to the prevalence of Laramide AFT dates in the range core include magmatism associated with the Colorado Mineral Belt and variable peak burial depths (Kelley & Chapin, 2004). The timing of cessation of Laramide contraction and attendant unroofing of the Precambrian crust varied across the Southern Rockies (Copeland et al., 2017; Tweto, 1975). Subsequent epeirogenic uplift and erosion (Abbott et al., 2022; Cather et al., 2012; Eaton, 2008) resulted in regional scale features such as the Rocky Mountain Erosion Surface (e.g., Chapin & Kelley, 1997; Epis & Chapin, 1974; Madole et al., 1987) and the modern topographic expression of the Southern Rockies.

2.2. Hematite (U-Th)/He Thermochronometry

(U-Th)/He thermochronometry is based on the interplay of ingrowth and diffusion of radiogenic He within minerals containing trace but measurable amounts of the parent radioisotopes 238 U, 235 U, 232 Th, and 147 Sm. Hematite (Fe₂O₃), one of the most common Fe oxides in Earth's crust, typically contains ppm concentrations of U and Th and normally excludes He during crystallization, making it suitable for (U-Th)/He thermochronometry (Bähr et al., 1994; Farley, 2018; Wernicke & Lippolt, 1993). The rate of He diffusion through crystals is strongly dependent on temperature and this relationship is commonly approximated by the *closure temperature*, or the temperature that separates open and closed system behavior with respect to He retention (Dodson, 1973). An important distinction between the hematite He system and the apatite and zircon (U-Th)/He (apatite He, zircon He) systems is the number of crystals analyzed within each aliquot. Apatite and zircon aliquots are individual, whole crystals that are tens to hundreds of μ m in width and have U, Th, and He contents sufficiently above blank levels. Hematite precipitates as polycrystalline aggregates of nm-to μ m-scale crystals that are too small to analyze individually (cf. Calzolari et al., 2020; Jensen et al., 2018) and thus hematite aliquots commonly contain numerous crystals of variable size. Each hematite crystallite in the aggregate acts as an individual He diffusion domain and the bulk (U-Th)/He closure temperature is determined by the size distribution of crystallites (Evenson

JENSEN ET AL. 4 of 22

15252027, 2023, 9, Downloaded from https

.wiley.com/doi/10.1029/2023GC010993,

Wiley Online Library on [16/09/2023]. See the Terms and Conditions

et al., 2014; Farley, 2018; Farley & Flowers, 2012; Jensen et al., 2018). Assuming a 10°C/Ma cooling rate and the He diffusion kinetics reported by Farley (2018), hematite He closure temperature ranges from ~40° to 255°C for tabular crystals with widths of 1 nm and 1 mm, respectively.

Hematite is a secondary phase of hydrothermal origin and precipitates over a range of depths and temperatures that can be above or below the hematite He closure temperature. Thus, hematite He dates can reflect different geologic processes depending on the precipitation conditions and post-formation thermal and mechanical history (Ault, 2020). Hematite He dates may record tectonic or erosional exhumation, hydrothermal mineralization, or He loss associated with friction-generated heat or hydrothermal fluid circulation during faulting (Ault et al., 2016; Jensen et al., 2018; McDermott et al., 2017; Moser et al., 2017). Grain size reduction during fault slip reduces the He diffusion domain size, causing aliquots to be more susceptible to diffusive He loss (Ault et al., 2015). Fluid inclusion microthermometry or apatite He thermochronometry, with a comparable closure temperature (~30°-120°C, Flowers et al., 2009), can help discriminate between data interpretations by informing the hematite crystallization conditions and ambient cooling history of the host rock, respectively. Interstitial phases within polycrystalline hematite aliquots may contribute U, Th, and/or He, or have different He diffusivity properties (Evenson et al., 2014). We targeted hematite with the highest possible purity for (U-Th)/He analysis to minimize the effects of other phases. We screened hematite aliquots with optical microscopy and SEM to characterize their purity, grain morphology and texture, and grain size distribution. Because hematite aliquots are three-dimensional (3D) volumes, microscopy techniques may not detect minor impurities that are either very small or that are present beneath the surface of aliquots. For this reason, we coupled microscopy-based screening with multi-element geochemical data to assess the purity of our hematite aliquots. These screening steps are crucial for valid interpretation of hematite He dates, especially when there is considerable dispersion within data sets.

3. Samples and Methods

3.1. Hematite Occurrence and Sampling Locality

We focus on a roadcut exposure along U.S. Route 285 (Figures 1 and 2), the same location of sampling site MR1 of Geissman and Harlan (2002). Here, the distinctive reddish-brown arkosic sandstone of the Pennsylvanian Fountain Formation dips moderately to the east and nonconformably overlies basement gneiss and schist coincident with the ~1.7 Ga Boulder Creek granodiorite (Peterman et al., 1968; Premo & Fanning, 2000). A zone of pervasive Fe oxide alteration parallels the nonconformity, extending into the basement rocks and overlying Fountain Formation. This alteration is expressed as a diffuse interstitial hematite matrix and cement, and is also present in greater concentrations in veins where subsequent localized fault slip produced minor, hematite-coated fault surfaces.

Hematite-altered basement rock is not suitable for hematite He analysis and we thus targeted the hematite fault surfaces because they contain polycrystalline hematite of sufficient thickness and purity. We collected two hematite-coated fault surfaces (samples A12-6, A12-10) and a sample of crystalline basement (sample A12-12) for hematite He and apatite He thermochronometry, respectively. Samples A12-6, A12-10, and A12-12 were collected ~100 m due west of the nonconformity (Figure 2a). Samples A12-6 and A12-10 are within a zone of Fe oxide alteration and A12-12 is on the margins of this zone. Six additional basement samples (285_1 to 285_6) were acquired at 1.25 m intervals along a basement transect at and away from the nonconformity for bulk magnetic susceptibility measurements, with sample 285_1 being the closest to the nonconformity and 285_6 being the farthest.

3.2. Scanning Electron Microscopy, Electron Probe Microanalysis, and Raman Spectroscopy

Hematite fault samples were prepared for chemical and textural characterization via SEM and EPMA. SEM and EPMA aliquots included standard thin sections, polished sample fragments mounted in epoxy, and unpolished (rough) fragments affixed to Cu adhesive tape. Thin sections were prepared with billets cut orthogonally to fault surfaces and parallel to the slickenline orientation. Polished and unpolished mounts comprise hematite fragments isolated from hand samples using fine-tipped tweezers and a Dremel tool and screened using a stereoscope. Polished mounts were coated with carbon to enhance conductivity and were analyzed via SEM in high-vacuum mode (<5e-5 torr). Rough, unpolished aliquots were analyzed with SEM under low vacuum at

JENSEN ET AL. 5 of 22

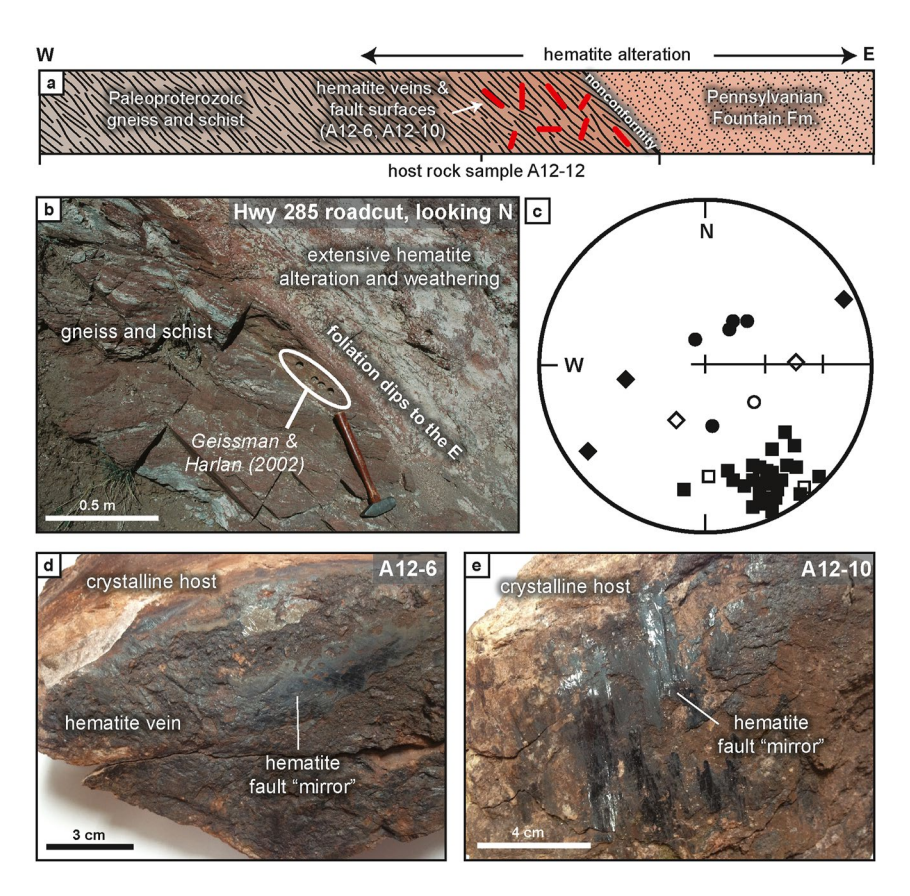


Figure 2. (a) Schematic showing geologic context of our sampling locality. Hematite fault surfaces A12-6 and A12-10 were sampled within the pervasive hematite alteration that parallels the contact between the basement and Fountain Formation. (b) Field photograph of one of the sampling locations of Geissman and Harlan (2002). (c) Equal area projection of directional paleomagnetic data previously collected from our study area, modified after Figure 4 of Geissman and Harlan (2002). Open and filled symbols plot on the upper and lower hemispheres, respectively. Squares: directions of linear segments of demagnetization trajectories as determined by principal components analysis; diamonds: normals to remagnetization circles used in analysis; circles: directions of magnetizations carried by magnetite in fresh schist and gneiss samples collected deeper below the nonconformity (d), (e) Photographs of hand samples A12–6 and A12-10.

variable pressures between 0.08 and 0.54 torr. SEM and EPMA analyses utilized accelerating voltages of 20–30 and 15 kV, respectively.

Secondary electron (SE) and backscattered electron (BSE) images of hematite samples were initially acquired at the Arizona Laserchron Center with a Hitachi 3400N SEM. Energy dispersive X-ray spectroscopy (EDS) elemental mapping was performed using an Oxford Instruments EDS detector on the Hitachi 3400N. EDS spot and map analyses were used to evaluate the degree of elemental heterogeneity within hematite samples, including candidate aliquots for (U-Th)/He dating. Subsequent SEM analyses of representative samples were performed at the Utah State University (USU) Microscopy Core Facility on a FEI Quanta 650 field-emission SEM, also paired with an Oxford EDS detector. We quantified the crystal size distribution of representative polycrystalline hematite aliquots by analyzing SEM images with imaging software ImageJ (Schneider et al., 2012). Crystals with clear boundaries were measured at and away from fault surfaces, with the goal of characterizing the breadth of textures and morphologies exhibited by hematite within our dated (U-Th)/He aliquots. For the estimation of the temperature sensitivity of dated aliquots, we use measured grain size distributions from portions of representative aliquots as proxies for the true grain size distribution within the 3D volume of dated aliquots. Geochemical maps of polished samples were acquired at the Lunar Planetary Lab of the University of Arizona via a Cameca SX100 EPMA.

Raman spectroscopic analyses were conducted using a Horiba LabRAM HR Evolution confocal Raman microscope system housed in the Mineral Microscopy and Spectroscopy Lab at USU to identify additional phases within representative hematite aliquots. The system was calibrated to the 520.7 cm⁻¹ band prior to spectra

JENSEN ET AL. 6 of 22

15252027, 2023, 9, Downloaded from https://agupubs.onlinelibrary.wiley.com/doi/10.1029/2023GC010993,

acquisition and includes a 532 nm Nd:YAG laser with a maximum output of 100 mW, a 75×50 mm Märzhäuser Wetzlar SCANplus motorized XYZ stage, and a Synapse charge-coupled device (CCD) camera. All spectra were processed and baseline corrected in the Horiba LabSpec 6 software package and collected using two accumulations of 15 s, a 600 gr/mm grating, a hole size of 100 μ m, and a neutral density filter of 5%–10%.

3.3. Hematite He, Apatite He, and Multi-Element Analyses

Hematite aliquots from fault samples A12-6 and A12-10 were analyzed for He, U, and Th following standard procedures for hematite (e.g., Reiners et al., 2014), which are described in more detail in Supporting Information S1 and S2 (Text S1 and Table S1). Briefly here, polycrystalline hematite aliquots were selected under a stereomicroscope using fine-tipped tweezers. We targeted hematite fragments that contained a natural polished surface from fault slip and no evidence of tool marks from the Dremel tool blade (Figure S2 in Supporting Information S1). The He contents of each aliquot were extracted by laser heating to temperatures of ~850°-900°C and quantified via quadrupole mass spectrometry. To monitor the potential volatilization of parent isotopes such as U during laser heating (Hofmann et al., 2020), we analyzed a subset of aliquots for U and Th only, hereafter referred to as "undegassed" aliquots. The U and Th contents of degassed and undegassed aliquots were determined via isotope dilution inductively coupled plasma mass spectrometry (ICP-MS). We do not apply an alpha-ejection (F_T) correction to hematite aliquots because we assume that alpha ejection from one crystallite is approximately balanced by alpha implantation from adjacent crystallites for three reasons. First, aliquots are dense polycrystalline hematite aggregates. Second, these aliquots were extracted from larger masses of hematite. Third, although aliquots contain slip surfaces, prior work from natural and experimental faults shows that slip surfaces develop within preexisting hematite veins or gouge, meaning that the "missing" side of the hematite fault surface likely comprised hematite as well (Ault et al., 2015; Calzolari et al., 2020; McDermott et al., 2017, 2021). Strong U and Th zonation over the length scales of tens to hundreds of microns (i.e., the size of our aliquots) can invalidate the assumption of alpha ejection balancing implantation and induce intrasample (U-Th)/He date dispersion.

The same solutions used for the U and Th measurements were reanalyzed by the same ICP-MS in a separate analytical session for other elements, including Fe, Al, Ti, and rare earth elements (REEs; Table S2 in Supporting Information S2), following procedures reported in Evenson et al. (2014) and Reiners et al. (2014). Fe, Al, and Ti were calibrated using 0.5–4 ppm standard solutions and less concentrated elements were referenced to 1–100 ppb standard solutions. Because our aliquots were not weighed prior to (U-Th)/He analysis, we report trace and minor elemental data in molar-based concentrations normalized to the amount of Fe within the solutions (μ mol analyte/mol Fe) as opposed to mass-based concentrations. Conversion to more commonly used mass-based concentration units (μ g analyte/g Fe₂O₃) assumes that Fe is present only in hematite and that the mass of any impurities is negligible compared to the hematite mass. We apply this conversion for comparison purposes in Table S1 in Supporting Information S2 and report both mass-based and molar-based effective uranium (eU) concentrations. The conversion factor is ~3 for converting molar-based to mass-based concentrations in hematite (Reiners et al., 2014).

We acquired apatite He data from basement sample A12-12 to provide a benchmark to compare with our hematite He results, considering the similarities in (U-Th)/He closure temperature between apatite and nano-to microcrystalline hematite (Figure S3 in Supporting Information S1). Whole apatite crystals were selected for (U-Th)/He dating based on crystal clarity, morphology, and lack of visible inclusions. Detailed grain measurements via stereomicroscope were used to calculate the F_T correction and the aliquot mass. Additional analytical details are in Supporting Information S1 and S2 (Text S1 and Table S3).

3.4. Bulk Magnetic Susceptibility

Powdered specimens from basement samples 285_1 through 285_6 were analyzed for bulk magnetic susceptibility at the UT Dallas Paleomagnetic and Rock Magnetic Laboratory using an AGICO MFKI-A susceptibility instrument attached to a CS4 high-temperature furnace. Susceptibility measurements were made continuously during heating and cooling steps in both air and inert (argon) atmospheres (Figure 3). Two splits were run from each sample, with one corresponding to air and the other argon. The split ran in air was reanalyzed a second time (Figure S4 in Supporting Information S1). Heating steps from all experiments were designed to meet or exceed the Curie and Néel temperatures of magnetite (~ 580 °C) and hematite (~ 680 °C), respectively.

JENSEN ET AL. 7 of 22

15252027, 2023, 9, Downloaded from https://agupubs

onlinelibrary.wiley.com/doi/10.1029/2023GC010993,

on [16/09/2023]. See the Terms

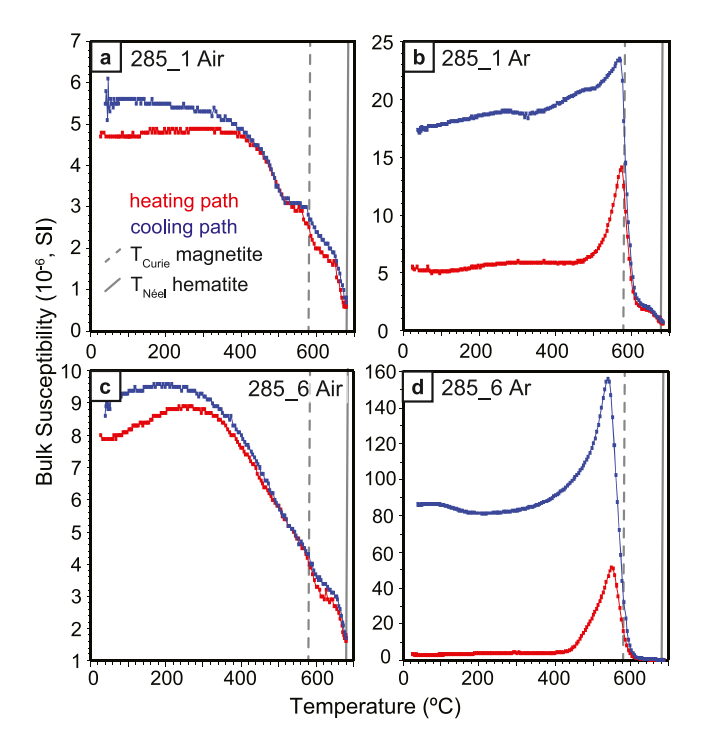


Figure 3. Bulk magnetic susceptibility measurements as a function of temperature from crystalline basement samples 285_1 (a, b) and 285_6 (c, d), which show that these samples do not fully lose their susceptibility until the Néel temperature of hematite is reached (solid gray line). Susceptibility measurements were made during sample heating (red path) and cooling (blue path), and within atmospheres composed of air (a, c) and argon (b, d).

4. Results

4.1. Hematite Textures and Morphology

Fault samples A12-6 and A12-10 comprise ~1–2 mm-thick hematite veins underlying striated slip surfaces that are approximately parallel to the orientation of vein mineralization (Figures 2d and 2e). Slip surfaces locally have a sub-mm, mirror-like veneer, which contrasts with the dull to earthy luster of the hematite vein material below. Weathering likely removed parts of a larger mirror-like slip interface, revealing the underlying vein and gneissic host rock. SEM shows that slip surfaces are hematite cataclasite with minor, comminuted quartz and feldspar clasts derived from the host rock (Figure 4). Hematite cataclasite in A12-10 also contains minor martite (the hematite pseudomorph after magnetite) clasts. Martite clasts are subhedral to euhedral. All martite clasts display a trellis pattern in cross-polarized reflected light, diagnostic of hematite forming along the octahedral crystallographic planes of the magnetite precursor. Fractured martite and host rock clasts are concentrated along the hematite-host rock contact and martite is observed within a subset of our A12-10 (U-Th)/He aliquots (Figure 4).

SEM of representative polycrystalline hematite aliquots reveal variable textures, grain morphologies, and grain sizes as a function of distance from the fault surface in both samples. Hematite grain size decreases toward the slip interface. Within \sim 5 µm of the fault surface, hematite particles are approximately equant, with grain half-widths as small as a few tens of nm (Figure 4). Away from this region, hematite grain size gradually increases to larger angular particles and locally fractured tabular plates up to \sim 1 µm in thickness. Across all representative aliquots, grains range in half-width from 0.03 to 1.16 µm when grain geometries are normalized to spherical radii with equivalent He closure temperature (Figure S5 in Supporting Information S1). The mean equivalent spherical radius of all measured crystallites (n = 764)

is $0.17 \mu m$. Oblique and plan views of the natural fault surface show a planar and qualitatively smooth interface with a series of parallel grooves comprising highly comminuted nanoparticles as well as void spaces that present views into the material immediately below the surface.

4.2. Hematite Geochemical Patterns

Differences in hematite fault surface geochemistry in aliquots from A12-6 and A12-10 delineate two data populations (Figure 5; Tables S1 and S2 in Supporting Information S2). Population 1 (P1; n = 36, including undegassed aliquots) and Population 2 (P2; n = 6) are primarily defined by differing concentrations of Th and light REEs La, Ce, Pr, Nd, and Sm. P1 aliquots exhibit REE concentrations ranging from a few tens to a few hundred µmol REE/mol Fe, and P2 aliquot REE concentrations are approximately five to nine times higher, with some aliquots reaching concentrations of several thousand µmol REE/mol Fe (Table S2 in Supporting Information S2). The overall trend of REE abundances mirrors the relative abundance of REEs within Earth's crust (Lide, 1997) with Ce as the most abundant REE and Sm as one of the least common (Figure S6 in Supporting Information S1). The anomalously high REE contents of P2 aliquots correlate to similar positive deviations in eU concentration (calculated as eU = [U] + 0.232*[Th], see Text S2 in Supporting Information S1 for more information). The parameter eU normalizes the concentration of parent isotopes U and Th based on the alpha productivity of their decay chains (e.g., Cooperdock et al., 2019; Shuster et al., 2006). P1 aliquots exhibit eU concentrations between 4.4 and 26.8 µmol eU/mol Fe and P2 aliquots yield higher eU ranging from 18.0 to 64.0 µmol eU/mol Fe. P1 and P2 aliquots share similar U contents but differ widely in Th, which results in higher eU and Th/U values in P2 aliquots. Undegassed aliquots from both A12-6 and A12-10 do not share the high REE contents of P2 aliquots but display eU and Th/U ranges that mostly encompass that of dated P1 aliquots and are thus assigned to P1.

Multi-element ICP-MS analyses of solutions also analyzed for hematite He dating, as well as SEM and EPMA analyses from representative thin sections, confirm hematite is the main constituent of the cataclastic material

JENSEN ET AL. 8 of 22

15252027, 2023, 9, Downloaded from https://agupubs.onlinelibrary.wiley.com/doi/10.1029/2023GC010993, Wiley Online Library on [16/09/2023]. See the Terms and Conditions (https://onlinelibrary.wiley.com/terms-and-conditions) on Wiley Online Library for rules of use; OA articles are governed by the applicable Creative Commons Licensea

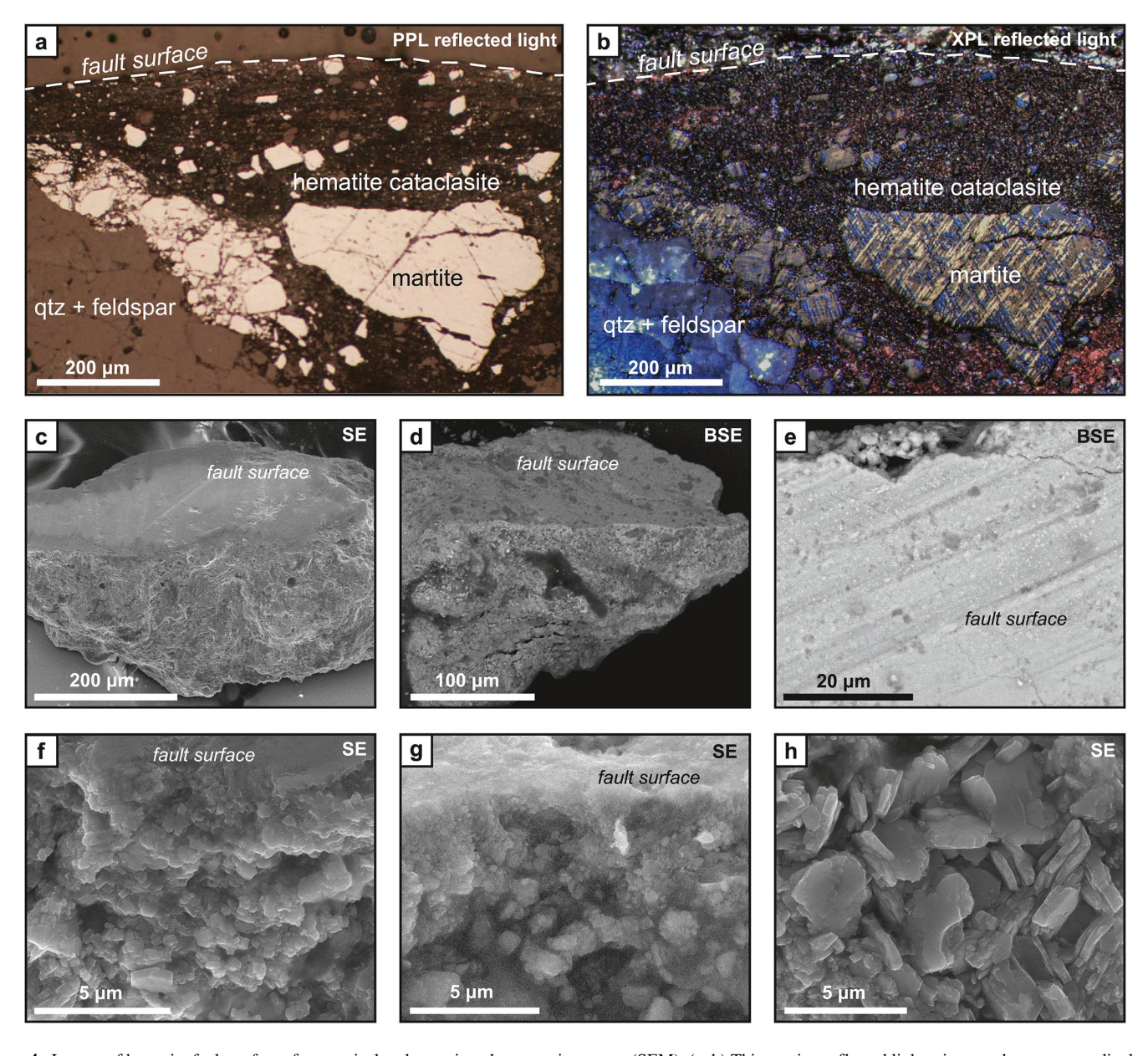


Figure 4. Images of hematite fault surfaces from optical and scanning electron microscopy (SEM). (a, b) Thin section reflected light micrographs cut perpendicular to the hematite-coated fault surface in (a) plane-polarized light (PPL) and (b) cross-polarized light (XPL). (c, d) Oblique SEM views of representative hematite aliquots that preserve the naturally polished fault surface and the underlying hematite matrix. (e) SEM plan view of hematite-coated fault surface, showing one set of striations. (f, g) SEM cross-sectional views of hematite fault surfaces and the underlying hematite cataclasite. (h) SEM image of undeformed plate-like hematite crystals away from the fault surface. SE = secondary electron image. BSE = backscattered electron image.

targeted for (U-Th)/He dating. Elevated light REE contents including Sm and Th in P2 aliquots imply the presence of light REE and Th-bearing phases other than hematite. SEM-EDS and EPMA analyses of A12-6 thin sections show such a phase with µm-scale crystals locally within fine-grained hematite cataclasite and that is concentrated near comminuted clasts of quartz and feldspar of the host rock (Figure 6 and Figure S9 in Supporting Information S1). This phase also comprises elevated F and variable amounts of Ca. P is not observed and indicates it is not monazite, a relatively common REE-bearing phosphate. Raman analyses yield compound spectra that show the distinctive bands of hematite mixed with the REE-bearing phase (Figure 6). A high intensity band in the 1,090 cm⁻¹ region implies that the REE-bearing phase is one of the fluorocarbonate minerals parisite or bastnäsite (also spelled bastnaesite), both of which are important REE ore minerals, with chemical forms Ca(REE)₂(CO₃)₃F₂ and REE(CO₃)F, respectively (Frost & Dickfos, 2007). Other impurities in

JENSEN ET AL. 9 of 22

1525/2027, 2023, 9, Downloaded from https://agupubs.onlinelibrary.wiley.com/doi/10.1029/2023GC010993, Wiley Online Library on [16/09/2023]. See the Terms and Conditions (https://onlinelibrary.wiley.com/terms-and-conditions) on Wiley Online Library for rules of use; OA articles are governed by the applicable Creative Commons Licensea

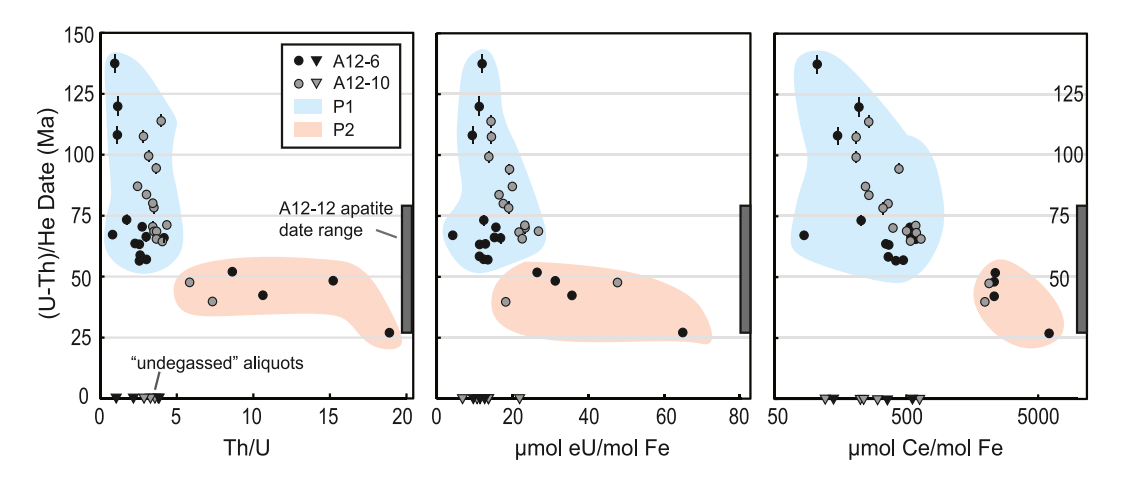


Figure 5. Hematite (U-Th)/He (hematite He) dates, categorized by population (P1 = blue, P2 = red) with their 2s analytical uncertainties as a function of Th/U, effective uranium (eU) concentration, and cerium (Ce) concentration. Symbols obscure any hematite He date uncertainty less than \sim 2 Ma. Concentration values are reported as molar ratios of the analyte referenced against mols of Fe. Triangles along the *x*-axis denote undegassed aliquots that monitor how laser heating may have affected aliquot chemistry (e.g., U loss). Gray bar = range of individual apatite (U-Th)/He dates from basement sample A12-12 shown for comparison.

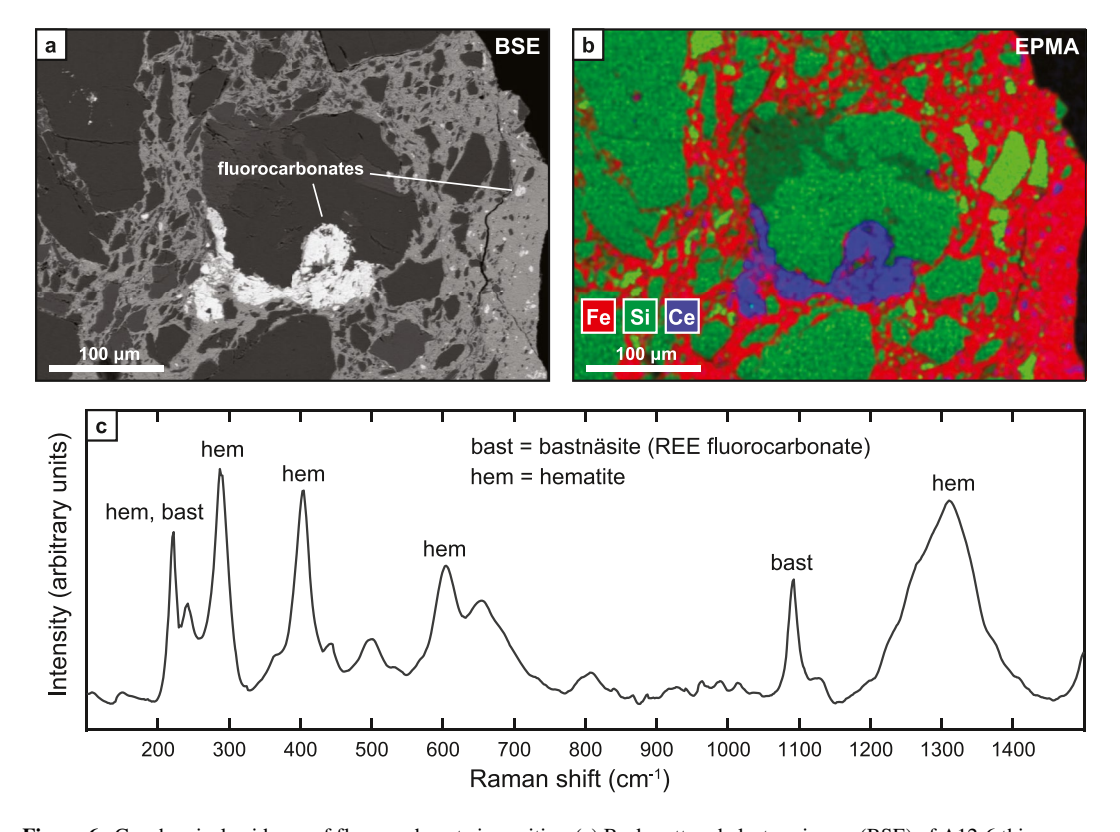


Figure 6. Geochemical evidence of fluorocarbonate impurities. (a) Backscattered electron image (BSE) of A12-6 thin section showing fluorocarbonates (white) suspended in a hematite matrix (light gray) and variably comminuted clasts of host rock silicate minerals (dark gray). Like hematite, fluorocarbonate grains show evidence of comminution (far right of image). (b) Elemental map from electron probe microanalysis (EPMA) shows the relative concentrations of Fe, Si, and Ce in the same area shown in (a). (c) Raman spectra collected from a grain of fluorocarbonate suspended in hematite with characteristic bands of hematite and fluorocarbonate minerals bastnäsite and parisite (Frost & Dickfos, 2007).

JENSEN ET AL. 10 of 22

5252027, 2023, 9, Downloaded from https://agupubs.onlinelibrary.wiley

on [16/09/2023]. See the Terms and Conditions

conditions) on Wiley Online Library for rules of use; OA

hematite cataclasite include a minor Ti-rich phase, which is present as clasts in the cataclasite and as anhedral patches suspended in the hematite matrix at the slip interface (Figure S7 in Supporting Information S1).

4.3. (U-Th)/He Data

Hematite He dates complement and define the same populations characterized by REE content (Table S1 in Supporting Information S2, Figure 5). Dated aliquots from P1 (n=27) yield a mean date of 80.1 ± 42.8 Ma ($\pm 2\sigma$ standard deviation of the mean), with individual dates ranging from 138 ± 4 Ma to 57.1 ± 1.7 Ma ($\pm 2s$ analytical uncertainty). P2 aliquots (n=6) yield exclusively Cenozoic hematite He dates from 51.8 ± 1.4 Ma to 27.0 ± 1.0 Ma ($\pm 2s$) and a mean date of 42.8 ± 16.2 Ma ($\pm 2\sigma$). Undegassed aliquots (n=9) show the same range in eU and Th/U as dated P1 aliquots. Overall, hematite He dates form a negative relationship with multiple parameters, including eU, Th/U, and REE abundance (Figure 5). Assuming all Fe derives from stochiometric Fe₂O₃ (hematite), the calculated hematite mass (a proxy for overall aliquot mass) of P1 and P2 aliquots ranges from ~10 to 230 µg (Table S1 in Supporting Information S2). We did not consider the alpha-producer ¹⁴⁷Sm in our reported hematite He dates. Although Sm was measured during our multi-element ICP-MS run, this is a different analytical session compared to measurements of U and Th and the effect of ¹⁴⁷Sm on the overall He budget in these samples is very small. Specifically, if ¹⁴⁷Sm measurements are included in the (U-Th)/He date calculation, the percentage difference in the calculated (U-Th)/He date is less than ~0.5% in all aliquots (Figure S8 in Supporting Information S1).

Individual apatite He dates from basement sample A12-12 (n = 8; Table S3 in Supporting Information S1) range from 78.5 \pm 3.0 Ma to 28.6 \pm 1.4 Ma (\pm 2s), with a mean date of 48.7 \pm 28.8 Ma (\pm 2 σ). Apatite grains are euhedral, transparent, and have low eU of ~100–300 ppb (ng/g). There is a weak relationship between apatite He date and grain size and no trend between apatite He date and eU (calculated as eU = [U] + 0.238*[Th] + 0.0012*[S m] where concentrations are mass-based; see Text S2 in Supporting Information S1).

4.4. Bulk Magnetic Susceptibility Results

Quasi-continuous thermomagnetic measurements of magnetic susceptibility in air from crystalline basement samples show a gradual decrease in susceptibility with temperature for heating and cooling steps below the Curie temperature of magnetite (\sim 580°C; Figure 3 and Figure S4 in Supporting Information S1). Heating and cooling curves are largely reversible at all temperature steps for samples where experiments are conducted in air, implying that sample mineralogy was stable during heating, as well as reheating in a second experiment. All samples measured in air, including repeat analyses, show sharp decreases in susceptibility at \sim 680°C. These results indicate that hematite is the dominant carrier of magnetization in these rocks. Minor magnetite is present in some samples, as shown by moderate decreases in susceptibility at \sim 580°C. Analyses carried out in argon atmosphere show reversible curve segments above 580°C and irreversible curve segments with an increase in susceptibility for temperatures less than \sim 580°C, representing the production of new magnetite. Measurements conducted in argon also show a decrease in susceptibility at heating steps near \sim 680°C that is diagnostic of hematite, although this signal is minor compared to that associated with the formation of new magnetite. Overall, samples from the \sim 6 m basement transect perpendicular to the nonconformity share a common magnetic mineralogy with magnetization attributed principally to hematite, consistent with the results of Geissman and Harlan (2002).

5. Discussion

5.1. Preliminary Interpretations of Comparative Hematite Data

Hematite-coated fault surfaces yield Cretaceous to Paleogene hematite He dates, significantly younger than the late Paleozoic hematite mineralization event identified by paleomagnetic data from the same sampling locality (Geissman & Harlan, 2002). The timing discrepancy between hematite He thermochronometry data and the interpreted age of the secondary, yet ancient magnetization (based on a correlation with estimated apparent polar wander paths for stable North America) highlights the potential differences in sensitivity of each of these dating techniques. Hematite He dates that are younger than the PCRS do not preclude that hematite, on what are now fault surfaces, initially formed during the late Paleozoic, coeval with hematite that is disseminated through the crystalline rocks. Cretaceous-Paleogene hematite He dates reasonably reflect post-formation, diffusive He loss in response to reheating during Mesozoic burial, immediately prior to Laramide exhumation. In contrast,

JENSEN ET AL. 11 of 22

.5252027, 2023, 9, Downloaded from https://agupubs.onlinelibrary.wiley.com/doi/10.1029/2023GC010993,

Wiley Online Library on [16/09/2023]. See the Terms

post-PCRS reheating episode(s) were not substantial enough to thermally unblock, over prolonged time periods, the late Paleozoic CRM. Hematite He dates from A12-6 and A12-10 are interpreted as cooling ages and the oldest hematite He date from each sample conservatively represents a minimum age of hematite formation.

Hematite He dates from P1 aliquots yield intrasample scatter in excess of tens of millions of years (Figure 5). Intrasample scatter of this magnitude likely reflects that cataclastic aliquots are characterized by variable grain size (i.e., diffusion domain size) distributions and thus closure temperatures, although we acknowledge that other sources of scatter may impact hematite He dates, including parent nuclide zonation and inclusions of other mineral phases. We do not interpret hematite He date scatter to reflect U loss from laser heating because of the overall similarity in Th/U and eU between dated and undegassed aliquots and because our aliquots were not heated to temperatures known to induce U volatilization (~1000°C; Hofmann et al., 2020). Even when U and Th heterogeneity between P1 aliquots is considered, U loss during laser heating is highly unlikely and/or has a minimal impact on hematite He dates (Figure S10 in Supporting Information S1).

Below, we first consider the temperature sensitivity of our hematite aliquots using SEM-based grain size analysis. We then use a suite of thermal history "forward" models that predict hematite He dates as a function of hematite grain size for prescribed thermal histories to evaluate whether grain size effects are the dominant source of scatter within P1 aliquots. The youngest hematite He dates of the entire data set are from P2 aliquots that display elevated Th and light REE. We assess the role that light REE and Th-bearing fluorocarbonate inclusions may play in contributing to these anomalously young (U-Th)/He dates.

5.2. Evaluating Grain Size Effects on Hematite He Dates

The observed range of hematite grain sizes within fault surface aliquots implies that individual aliquots will differ in overall temperature sensitivity. This introduces substantial, but potentially predictable, scatter into our hematite He data set and, in this section, we consider grain size effects on our hematite He dates and data interpretations. Assuming that individual crystals define He diffusion domains and a homogenous distribution of U and Th at the spatial scale of aliquots, the temperature sensitivity of polycrystalline aliquots is governed by the crystal size distribution and the volume fraction of each individual crystal relative to the aliquot volume. Polycrystalline aliquots with a greater volume fraction of large grains are expected to have a higher bulk closure temperature and yield older hematite He dates than aliquots with a comparatively smaller portion of large grains. The difference in closure temperature between individual hematite aliquots from fault surfaces can be substantial because the grain size variability in naturally precipitated hematite and subsequent comminution during fault slip causes grain sizes to evolve and decrease through time.

To evaluate the influence of the grain size distribution on hematite He dates, we first calculate closure temperature following the method of Dodson (1973) and by assuming the He diffusion kinetics of Farley (2018), a 10°C/Ma cooling rate, and a spherical crystal geometry. The half-widths of grains displaying tabular, plate-like geometries were converted to half-widths of spheres with identical closure temperature by multiplying by a factor of 2.5, a relationship derived from the closure temperature equation and grain geometry constants (55 for a sphere, 8.7 for a plane sheet) of Dodson (1973). The mean closure temperature of all measured grains (n = 764) is $83 \pm 15^{\circ}$ C $(\pm 2\sigma$ standard deviation of the mean) and the range is from 67 to 111°C. Because polycrystalline aliquots contain mixtures of grain sizes between the minimum (0.03 μm) and maximum (1.17 μm) observed crystal radii, the true closure temperature variation among dated aliquots should be less than that of individual crystals. The closure temperature range of individual crystals within hematite aliquots partially overlaps with the closure temperature of the apatite He (~30–120°C; Flowers et al., 2009) and AFT systems (~90–120°C; Ketcham et al., 2007). Low eU apatite grains from A12-12 that experienced rapid Laramide cooling likely have a closure temperature marginally lower than most of our hematite He aliquots (\sim 60–65 $^{\circ}$ C; Flowers et al., 2009). Our apatite He dates are younger than most hematite He dates and previously reported >100 Ma AFT dates from nearby localities are older than the bulk of our hematite He dates (Figure 1b; Kelley & Chapin, 2004). These relationships are consistent with the notion that the estimated temperature sensitivity of our polycrystalline hematite He aliquots is broadly between the apatite He and AFT systems and that hematite He dates reflect variable degrees of He loss since hematite formation.

We next use the forward modeling capabilities of the software package HeFTy (Ketcham, 2005) to evaluate (a) if grain size variation among hematite aliquots can explain the observed (U-Th)/He date dispersion in P1 and (b) the plausibility of a late Paleozoic formation age for hematite mineralization coeval with diffuse hematite alteration documented on the basis of paleomagnetic data (Geissman & Harlan, 2002). Hematite aliquots from

JENSEN ET AL. 12 of 22

1525/2027, 2023, 9, Downloaded from https://agupubs. onlinelibrary.wiley.com/doi/10.1029/2023GC010993, Wiley Online Library on [16/09/2023]. See the Terms and Conditions (https://onlinelibrary.wiley

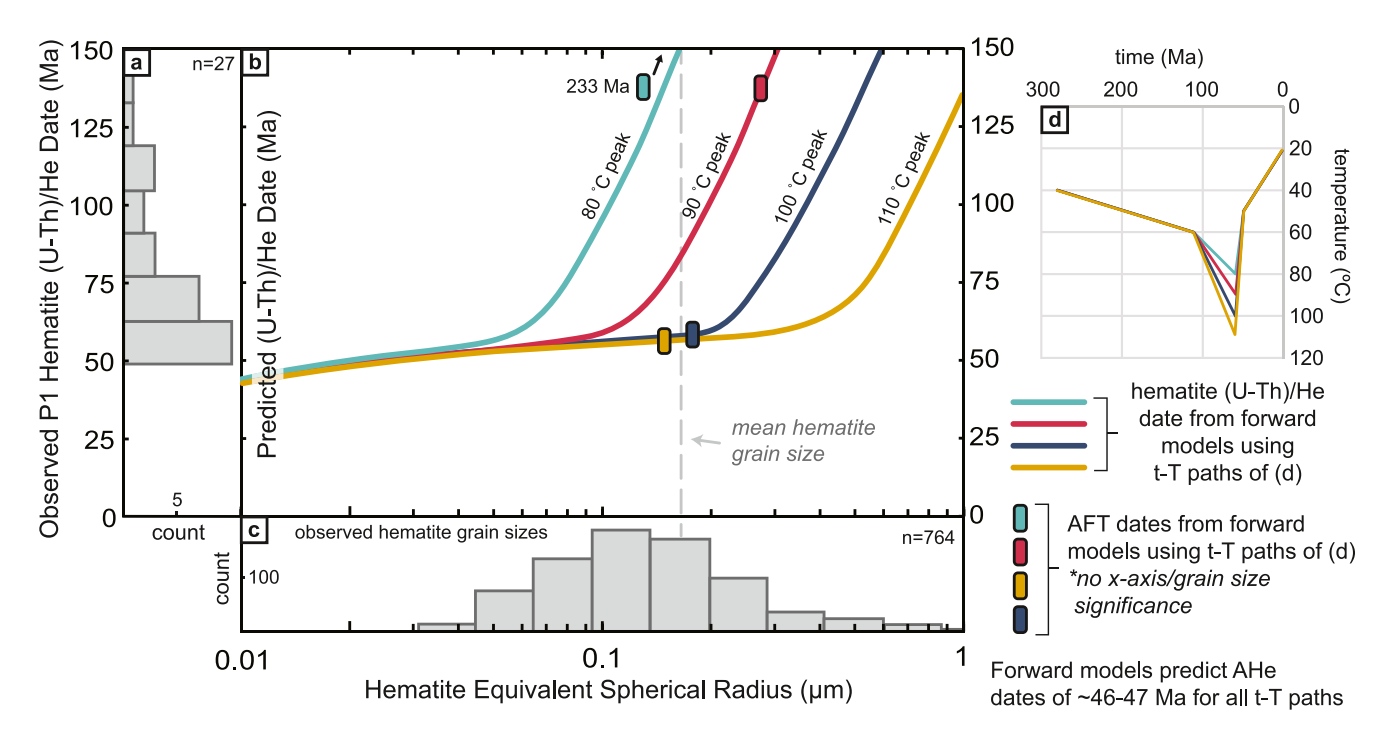


Figure 7. Comparison of forward modeling predictions to observed hematite (U-Th)/He (hematite He) dates and grain size measurements. (a) Observed population 1 (P1) hematite He dates (n = 27). (b) Predicted hematite He dates scale with hematite grain size. Each model curve corresponds to a time-temperature (t-T) path shown in (d). Predicted apatite fission-track (AFT) results are shown on the top of their associated hematite model curves that assumed the same t-T history (AFT symbols have no x-axis significance). (c) Log-scale histogram of the size distribution of all measured hematite grains from scanning electron microscopy (SEM) investigations (n = 764). The gray dashed line is mean grain size from all measurements. (d) t-T paths used in forward models, which vary the magnitude of reheating from Late Cretaceous/early Paleogene burial. Predicted apatite (U-Th)/He (AHe) dates from the t-T paths of (d) are listed in the lower right legend.

P2 are not considered in this modeling exercise because we interpret that these aliquots contain eU-rich fluorocarbonate, which modified the He production and diffusivity characteristics of these aliquots, as discussed in the next section. Forward models employ the hematite He diffusion kinetics of Farley (2018) and assume a spherical diffusion domain geometry. We use HeFTy to generate hematite He dates that span the range of observed hematite crystal sizes and compare the predicted date trends with our hematite He data set. Models assume simple time-temperature (t-T) histories that begin at 280 Ma and 40°C, which reflects the approximate timing of hematite mineralization in the shallow crust during the PCRS and after deposition of the Fountain Formation. A simple burial path connects the formation t-T constraint to peak burial temperatures at 60 Ma, with an inflection point at 110 Ma representing the increase in burial rate implied by thick, upper Mesozoic sedimentary deposits in this area (Scott, 1972). Models include rapid cooling to moderate temperature (50°C) at 50 Ma to reflect Laramide unroofing, consistent with our apatite He results, followed by cooling to surface temperature (20°C) by present day. We vary peak temperatures at 60 Ma from 80° to 110°C to illustrate the sensitivity of hematite crystals to these t-T conditions. We do not consider shear heating in our models (cf. Armstrong et al., 2022) because hematite aliquots do not exhibit grain morphologies diagnostic of temperatures that might induce partial to complete He loss (Ault et al., 2015, 2019; McDermott et al., 2017, 2023; Odlum et al., 2022). Details of our thermal history model setup are included in Table S4 in Supporting Information S2.

Forward models produce hematite He date-grain size trends that span the observed date dispersion within P1 aliquots (\sim 138–57 Ma; Figure 7). Model outcomes illustrate that only a modest difference in grain size distribution among aliquots is required to produce the observed dispersion. For example, in the 90°C peak burial scenario, the observed hematite He date span in P1 aliquots is encompassed by grains with radii ranging from 0.09 to 0.28 μ m (corresponding to a closure temperature range of 84°–99°C), which is well within the spread of grain sizes observed within representative polycrystalline aliquots (Figure 7 and Figure S5 in Supporting Information S1). For all simulated thermal histories, grain sizes corresponding to the bulk closure temperature of polycrystalline aliquots must differ by a factor of \sim 3–4 to reproduce the observed hematite He date scatter. In addition, predicted hematite He date-grain size trends show that the grain sizes required to retain pre-Laramide hematite He dates increase with increasing peak burial temperature during the latest Cretaceous/earliest Paleogene.

JENSEN ET AL. 13 of 22

15252027, 2023, 9, Downloaded from https://agupubs

onlinelibrary.wiley.com/doi/10.1029/2023GC010993,

The crossover between fully reset and partially reset grains occurs within the spectrum of observed grain sizes for all t-T paths (Figure 7). One implication of this observation is that hematite aliquots of this size range are mostly insensitive to pre-Laramide events, including initial hematite mineralization. For instance, predicted hematite He dates for the mean observed grain size are either fully reset (in the 100° and 110°C scenarios) or partially reset (in the 80° and 90°C scenarios) and do not retain formation ages, even in the coolest t-T scenario (Figure 7). Therefore, the hematite He data and our thermal models permit hematite mineralization in the early Permian as is postulated by Geissman and Harlan (2002), but models of earlier hematite formation (pre-ARMO) are also permissible when considering only our reported hematite He results. We favor hematite formation and the acquisition of secondary, yet ancient magnetization in the late Paleozoic, considering the independent paleomagnetic evidence (Geissman & Harlan, 2002).

We compare predicted hematite He, AFT, and apatite He dates from our forward thermal models to our observed hematite and apatite He dates and previously published >100 Ma AFT dates from <20 km away (Kelley & Chapin, 2004) to assess peak burial temperatures during the Late Cretaceous/early Paleogene. Modeled apatite He dates are fully reset in every t-T scenario and are thus insensitive to different peak burial temperatures. Although predicted apatite He dates (46-47 Ma) closely match the mean apatite He date (~48.7 Ma), forward models do not reproduce the observed apatite He data. (U-Th)/He date dispersion in these basement-hosted, low-eU apatite grains of similar size may reflect variable amounts of high eU, grain-bounding phases that were removed during sample processing (Murray et al., 2014; Spiegel et al., 2009). In contrast, models predict AFT dates that are variably reset, depending on peak burial temperature. Specifically, fission tracks in apatite are largely annealed during the latest Cretaceous/earliest Paleogene at 100° and 110°C peak temperatures, but cooler peak burial temperatures (80° and 90°C) yield AFT dates >100 Ma, consistent with our expectation of pre-Laramide AFT dates. In addition, the 100° and 110°C model scenarios predict pre-Laramide hematite He dates for grain sizes that are far larger than the mode and mean of the observed grain size population. For these reasons, we prefer the 90°C path because of the overall agreement between the observed grain size population with the predicted distribution of grain sizes that correspond to the observed hematite He date range. The 90°C scenario implies a geothermal gradient of ~21°C/km, assuming a sedimentary thickness of 3.4 km (Pennsylvanian through latest Cretaceous sedimentary column; Scott, 1972) and a mean surface temperature of 20°C. This is lower than the modern temperature gradients observed in the Denver Basin (Kelley & Blackwell, 2002), but is not unreasonable in the active foreland sedimentary basin of the Late Cretaceous Western Interior Seaway (e.g., Schütz et al., 2018).

The timing of hematite grain comminution with respect to peak burial and residence in the partial He retention zone (PRZ) impacts the He budget and hematite He date from each aliquot. HeFTy forward models assume hematite He domain size in samples A12-6 and A12-10 remained constant through time. SEM images support variable grain comminution of preexisting hematite vein material during fault slip (Figure 4). Grain comminution modifies the He domain size distribution and lowers overall aliquot He retentivity (i.e., lowers the bulk closure temperature). We suggest hematite aliquots were variably comminuted and much of this fault-related grain size reduction occurred prior to or was coincident with peak burial and Laramide exhumation, permitting hematite He dates from aliquots with different grain size distributions to diverge. This scenario would result in a positive relationship between hematite He date and grain size because coarser-grained aliquots would preserve older hematite He dates than aliquots with comparatively higher magnitudes of grain comminution. If the grain size reduction that produced the observed grain size distribution occurred after peak burial (post-50 Ma), then any He loss after this period would be negligible because most grains, as observed today, are sufficiently large to be retentive of radiogenic He at the near-surface temperatures experienced during this portion of the t-T history (~20°-50°C). In this scenario, hematite He dates would be decoupled from observed grain sizes and imply higher peak burial temperatures that were hot enough to induce partial to complete He loss in larger, pre-deformation grains. Independent evidence from the AFT system instead suggests minimal grain size reduction in hematite aliquots since peak burial because temperatures of >100°C would fully anneal fission tracks and yield Laramide AFT dates, which are not observed. Although we lack quantitative grain size measurements from each dated aliquot, grain size populations from representative samples show sufficient variability to account for the observed hematite He date dispersion in P1 aliquots.

JENSEN ET AL. 14 of 22

15252027, 2023, 9, Downloaded from https://agupubs

5.3. Geochemical Controls on Hematite He Dates

Trace differences in grain chemistry and mineralogy have the potential to affect the He retentivity of hematite, especially that of P2 aliquots. P2 aliquots displaying elevated Th/U, eU, and light REE are associated with the youngest He dates and mostly fall outside the ranges in geochemistry measured in undegassed aliquots, notably with Th/U (Figure 5; Tables S1, S2 in Supporting Information S2). Dated P2 aliquots with distinctly higher Th/U than undegassed aliquots may indicate U loss during He extraction and measurement, causing aliquots to appear too old (Danišík et al., 2013; Hofmann et al., 2020; Vasconcelos et al., 2013). We do not suspect U loss due to laser heating in P2 aliquots because these aliquots are anomalously young (as opposed to being anomalously old) and because they show higher total Th than P1 aliquots (Table S1 in Supporting Information S2). The observed Th/U increase is most likely related to an increase in Th from mineral impurities. We interpret geochemical anomalies, including elevated Th, to reflect variable incorporation of the Th-bearing fluorocarbonate minerals parisite and bastnäsite (Figure 6 and Figure S9 in Supporting Information S1). The fact that none of the undegassed aliquots yield geochemical patterns akin to P2 aliquots is considered coincidental.

Most of the hematite He date dispersion among P2 aliquots reflects differences in geochemistry rather than differences in grain size distribution. SEM images of hematite cataclasite containing fluorocarbonate show no discernible difference in hematite grain size distribution from other regions where fluorocarbonate is absent. In addition, when using REE concentration as a proxy for fluorocarbonate contents in each aliquot, a general negative relationship exists between hematite He date and fluorocarbonate concentration (Figure 5). This pattern also extends to P1 aliquots, suggesting that fluorocarbonate impurities together with grain size differences influence P1 hematite He dates. Aliquot A12-6_H2 from P1 yields a ~67.2 Ma date and has the lowest Ce concentration of the entire data set, making it a notable outlier of the overall hematite He date-REE relationship (Table S2 in Supporting Information S2) and one that helps reinforce the interpretation that grain size differences are the primary control on hematite He dates in P1 aliquots.

The observed relationship between increasing amount of fluorocarbonate and decreasing hematite He dates leads us to speculate on the processes that underpin it. Parisite and bastnäsite can form as primary magmatic minerals or as alteration products from fluid-mediated, dissolution-reprecipitation reactions and minor accumulations of both genetic types are reported in nearby basement-hosted pegmatites and mining districts (Eckel, 1961; Li et al., 2021; Raschke et al., 2021). In A12-6 thin section, fluorocarbonate is a secondary mineral, variably dispersed within the hematite, with greater accumulations observed near comminuted clasts of the host rock material (Figure 6 and Figure S9 in Supporting Information S1). Because clasts of fluorocarbonate are observed within the fault surface cataclasite, we infer that the fluorocarbonate is as old as the hematite mineralization and thus rule out a late, post-Laramide phase of fluorocarbonate mineralization that would reduce hematite He dates from aliquots containing fluorocarbonate.

A potential explanation for why P2 aliquots are comparatively young relates to the He retentivity of the eU-rich fluorocarbonate. Radiogenic Pb in fluorocarbonate is susceptible to fluid mobilization (Li et al., 2021), but the diffusivity characteristics of radiogenic He in these minerals are unknown. The observed negative association between fluorocarbonate concentration and (U-Th)/He date suggests that fluorocarbonate has low He retentivity at near-surface temperatures, resulting in (U-Th)/He closure temperatures much lower than that of similarly sized hematite grains (i.e., <80°C). Our interpretation of low He retentivity in the fluorocarbonate is applicable to grain clusters that are larger than tens of microns, which is an approximation of alpha-stopping distances in most minerals (Ketcham et al., 2011). Accumulations smaller than this threshold would lose a majority of their He budget through alpha ejection to surrounding phases and this He loss would not be fully balanced by alpha implantation, considering the eU of the fluorocarbonate is greater than that of the surrounding hematite and host silicates (Figure S9 in Supporting Information S1 and Table S2 in Supporting Information S2). Ejected He implanted into hematite would be mostly retained at near-surface temperatures, but any He implanted into quartz or feldspar would be rapidly lost by diffusion even at surface temperatures because of low He retentivity (Lippolt & Weigel, 1988; Shuster & Farley, 2005). Taken together, we suggest that aliquots with fluorocarbonate inclusions sufficiently larger than typical alpha stopping distances would be associated with higher REE concentrations and yield younger hematite He dates than aliquots with lower REE concentrations or that have mostly fine-grained fluorocarbonate clusters.

JENSEN ET AL. 15 of 22

15252027, 2023, 9, Downloaded from https://agupubs.onlinelibrary.wiley.com/doi/10.1029/2023GC010993, Wiley Online Library on [16/09/2023]. See the Terms and Conditions (https://onlinelibrary.

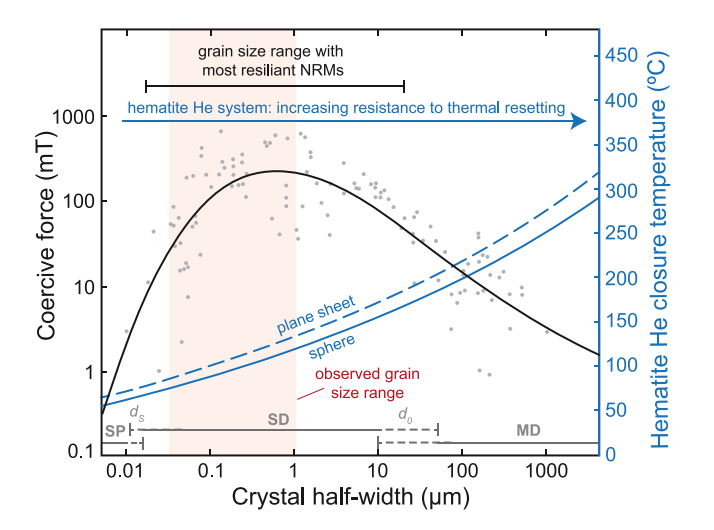


Figure 8. Coercivity (i.e., the resistance to demagnetization) of hematite as a function of grain size (modified after Özdemir & Dunlop, 2014). Secondary y-axis shows hematite (U-Th)/He (hematite He) closure temperature as a function of the same range of hematite grain size. Shaded red region = grain size range observed in our hematite cataclasite, implying that these grains have relatively high potential to preserve magnetizations but have relatively low (U-Th)/He closure temperatures. Closure temperature calculations assume the He diffusion kinetics of Farley (2018), spherical (solid blue line) and plane sheet (dashed blue line) domain geometries, and a cooling rate of 10° C/Ma. NRM = natural remanent magnetization. SP = superparamagnetic. SD = single domain. MD = multidomain. d_s = critical grain size where the magnetic behavior changes from SP to SD. d_o = critical grain size where the magnetic behavior changes from SD to MD.

6. Comparison Between Paleomagnetic and (U-Th)/He Data and Approaches

We compare paleomagnetic and hematite He data to assess the compatibility of these systems and the utility of hematite He analyses to provide independent, geochronologic constraints on primary and/or secondary components of NRMs that are geologically stable. In this case study, we specifically investigated whether hematite He dates record the same late Paleozoic, Fe oxide mineralization age determined by prior paleomagnetic results from the same locality in the Colorado Front Range (Geissman & Harlan, 2002). Our documented incongruity between hematite He and paleomagnetic data sets from this locality highlights important differences in sensitivity and sampling requirements between the two systems that have the potential to hamstring future studies seeking to date primary and secondary magnetizations with hematite He chronometry.

First and foremost, the Fe oxide phase being dated should be the same phase that the carries the bulk of the observed NRM. In our example, new and prior rock magnetic analyses confirm that disseminated secondary hematite mineralization resulted in the dominant magnetization carrier in these rocks (Figure 3 and Figure S4 in Supporting Information S1). However, the diffuse hematite alteration zone sampled by Geissman and Harlan (2002) is not suitable for hematite He analyses because of the pervasiveness of non-Fe oxide, unretentive phases in the crystalline basement that would render hematite He dates from such material uninterpretable. To minimize effects from other phases, we acquired (U-Th)/He dates from hematite that was sufficiently concentrated at discrete fault surfaces localized within hematite veins. We interpret that the diffuse hematite alteration and hematite veins are genetically related, supported by hematite He data patterns and thermal history simulations, although we acknowledge the vein mineralization age could differ from the inferred age of the late Paleozoic remanent magnetization characteristic of this locality.

Second and related, hematite grain size impacts the temperature sensitivity of the hematite He system and its magnetic behavior (i.e., domain structure, as reflected in coercivity values and other rock magnetic properties). Diffuse alteration and vein material exhibit grain sizes where individual crystals are expected to act as single magnetic domains (Figure 8). Thus, the definition of what constitutes a "domain" is consistent from both paleomagnetic and He diffusion perspectives (Banerjee, 1971; Farley, 2018; Kletetschka & Wasilewski, 2002; Özdemir & Dunlop, 2014). In very coarse-grained hematite, however, magnetic domains from individual grains transition from single to multidomain behavior. For grains larger than the critical size, d_s , which describes the shift between superparamagnetic and single domain behavior (Banerjee, 1971), the temperature sensitivities of the hematite He and paleomagnetic systems show opposing relationships with grain size (Figure 8). For grains with half-widths between ~0.03 and 10 μm, hematite peaks in coercivity and magnetization are carried exclusively within grains that are single domain (Özdemir & Dunlop, 2014). Magnetic unblocking temperatures for grains of this size range are variable (Dodson & McClelland-Brown, 1980) but are universally much greater than (U-Th)/He closure temperatures (Figure 8). Thus, hematite He dates from this crystal size range are more prone to thermal resetting than hematite-hosted NRMs (ignoring chemical reactions that can be associated with temperature increases). In the (U-Th)/He system, hematite crystals with half-widths >100 μm are less susceptible to thermal resetting, having relatively high closure temperatures that exceed that of the upper end of the zircon He system (i.e., 225°C; Guenthner et al., 2013). Hematite grains of this size range are greater than the critical magnetic domain size, do, which defines the onset of magnetic multidomain behavior in hematite. Magnetizations in multidomain grains are generally of lower intensity and lower coercivity, and thus more susceptible to overprinting than remanence carried by single domain grains. The contrasting effects of hematite grain size on the paleomagnetic and (U-Th)/He systems underscores an important point: for any given grain size, these systems

JENSEN ET AL. 16 of 22

.5252027, 2023, 9, Downloaded from https://agupubs.onlinelibrary.wiley.com/doi/10.1029/2023GC010993,

are unlikely to record the same geologic event, especially if hematite experienced any post-formation reheating at relatively low temperatures from burial or hydrothermal fluids.

Although our hematite He dates are far younger than the interpreted timing of CRM acquisition, they still yield valuable constraints on the timing of initial hematite formation and CRM acquisition. Pre-Laramide hematite He dates provide an independent check on the age of the CRM and effectively rule out a complete overprint by a Late Cretaceous to early Paleogene CRM, a plausible scenario considering that sedimentary rocks elsewhere in the Southern Rocky Mountains and vicinity show evidence of remagnetization at this time (Geissman et al., 1991; Pivarunas & Meert, 2019). In addition, (U-Th)/He dates support initial hematite crystallization and CRM development in the late Paleozoic when modeled to account for post-formation diffusive loss of He that likely occurred during late Mesozoic burial and reheating. Evolving (U-Th)/He domain sizes, through grain size reduction that accompanied cataclasis, contributed to hematite He dates being younger than a likely late Paleozoic formation age. We anticipate that intact vein material, free of fault-related deformation, would display the same CRM as carried by the host rocks with diffuse hematite alteration. Depending on the magnitude of grain rotations from cataclastic flow, any vein material that shows signs of fault movement and deformation would likely pass a micro-conglomerate test, if possible to perform, and provide further evidence that the CRM was acquired before fault initiation. This may not hold true for fault surfaces developed on secondary hematite from other localities that display textural and geochemical evidence of flash heating and/or recrystallization (e.g., Ault et al., 2019; McDermott et al., 2017, 2023), as these surfaces are more likely to acquire new localized magnetizations related to the timing of fault slip as opposed to initial vein formation.

A subset of basement samples examined by Geissman and Harlan (2002) exhibit a partial remanence overprint (see Section 2.1; Figure S1 in Supporting Information S1). If this reflects a partial thermoviscous remanent magnetization (pTVRM) carried by hematite, it may be reasonably connected to the same Late Cretaceous/early Paleogene reheating episode invoked by our thermal history models that can explain our hematite He data patterns (Figure 7d). Considering the hematite blocking curves of Pullaiah et al. (1975), a heating episode of this magnitude and duration could produce a partial overprint with laboratory unblocking temperatures consistent with those observed in some samples displaying the pTVRM (~400–500°C; Figure S1 in Supporting Information S1). However, we prefer to not interpret this partial overprint in the context of our hematite He data, considering it (a) is not observed in all samples with the late Paleozoic CRM, (b) shows variability in direction, (c) is not directionally distinguishable from the modern field, and (d) may be the product of a non-thermal (e.g., chemical) process.

Future studies seeking to integrate paleomagnetic and (U-Th)/He data sets from Fe oxides must first consider the important caveats and limitations of pairing these two approaches. The structure, morphology, and geochemical context of magnetic and He diffusion domains through time, along with the post-formation thermal history, are all variables that factor into whether magnetizations and (U-Th)/He dates record the same geologic event. In many cases, hematite (and Fe oxide more broadly) He dates will not have an explicit temporal connection to the acquisition of the strongest component of NRM because of differences in system sensitivity, even when the material being (U-Th)/He dated is the exact same material that yields a geologically stable and coherent magnetization. Hematite He dating requires sufficiently pure aliquots free of non-retentive phases, a condition that does not characterize most rock types that are otherwise typically high-quality paleomagnetic recorders (e.g., hematite-cemented, fine grained siliciclastic rocks). Even in cases where samples have sufficiently pure hematite accumulations, hematite is often fine grained to where radiogenic He is fully retained only at low to moderate temperatures much lower than the magnetization unblocking temperatures of the same grains (Dodson & McClelland-Brown, 1980; Garcia et al., 2018; Reiners et al., 2014). Hematite samples that conform to the limitations described above and that are associated with simple formation and thermal histories (e.g., secondary hematite samples that remained at near-surface temperatures less than ~60 °C) thus represent the optimal use case of combined paleomagnetic and (U-Th)/He investigations. In some scenarios, a well-grouped pTVRM carried by magnetic domains with low geologic unblocking temperatures that are similar to hematite He closure temperatures may yield insight into the magnitude and duration of overprinting thermal processes that also partially to fully reset the hematite He system (Dunlop et al., 1997; Pullaiah et al., 1975). Alternatively, robust hematite He data with complementary grain size distribution information have the potential to inform a thermal history that produces a pTVRM. We emphasize that, in these circumstances, complexities in paleomagnetic and hematite He data patterns represent compatibility between these two systems and an opportunity for future research.

JENSEN ET AL. 17 of 22

15252027, 2023, 9, Downloaded from https://agupubs.onlinelibrary.wiley.com/doi/10.1029/2023GC010993, Wiley Online Library on [16/09/2023]. See the Terms

18 of 22

7. Conclusions

Minor hematite-coated fault surfaces collected below a regional nonconformity along the Front Range of Colorado yield hematite He dates that span from the Early Cretaceous to the late Paleogene. Intrasample hematite He date dispersion reflects variable He loss between polycrystalline hematite aliquots with differing hematite grain size distributions. Aliquots yielding (U-Th)/He dates older than the Laramide orogeny are interpreted to be associated with larger grain size distributions, having higher overall He retentivity compared to aliquots with a higher proportion of smaller, cataclastic, and less He retentive grains that were fully reset by Mesozoic burial. We interpret low He retentivity in aliquots with fluorocarbonate impurities because these aliquots exhibit the youngest hematite He dates in the data set. Thermal history forward models of (U-Th)/He data support initial hematite mineralization and remagnetization of most of these crystalline rocks in the late Paleozoic, consistent with reported paleomagnetic data, although the upper bound on the modeled hematite formation age is unconstrained.

Prior work showed that basement rocks at our sampling locality, along with crystalline rocks at several additional localities in the region, are characterized by a well-grouped, late Paleozoic CRM carried by hematite. This age constraint derived from paleomagnetism was a primary motivation of this study, where we evaluate the compatibility between the (U-Th)/He and paleomagnetic systems in secondary hematite. Because the age of hematite-carried magnetizations is often unclear, independent age constraints on hematite formation from the (U-Th)/He system have the potential to resolve uncertainties and improve interpretations in paleomagnetic studies. However, hematite He dates from our case study are collectively much younger than the late Paleozoic magnetization event, highlighting that hematite grains capable of recording strong, coherent magnetizations are susceptible to diffusive He loss because of their relatively small grain size. The differing sampling requirements for paleomagnetic and (U-Th)/He analyses represent another challenge in combining these two systems. For example, rocks with diffuse hematite mineralization (e.g., hematite cements in sedimentary rocks) are typically not appropriate candidates for (U-Th)/He dating because of complexities introduced by phases that are not retentive of radiogenic He (e.g., quartz and feldspar). We thus suggest that it is unlikely for hematite He dates to be temporally linked to the acquisition of remanent magnetizations, except for rocks with well-characterized pTVRM or that experienced relatively cool and simple thermal histories.

Data Availability Statement

All information in the Supporting Information is archived and freely available at figshare.com (https://doi.org/10.6084/m9.figshare.22572883.v1).

References

- Abbey, A. L., Niemi, N. A., Geissman, J. W., Winkelstern, I. Z., & Heizler, M. (2018). Early Cenozoic exhumation and paleotopography in the Arkansas River valley, southern Rocky Mountains, Colorado. *Lithosphere*, 10(2), 239–266. https://doi.org/10.1130/L673.1
- Abbott, L. D., Flowers, R. M., Metcalf, J., Falkowski, S., & Niazy, F. (2022). Post-Laramide, Eocene epeirogeny in central Colorado—The result of a mantle drip? Geosphere, 18(4), 1223–1246. https://doi.org/10.1130/ges02434.1
- Armstrong, E. M., Ault, A. K., Bradbury, K. K., Savage, H. M., Polissar, P. J., & Thomson, S. N. (2022). A multi-proxy approach using zircon (U-Th)/He thermochronometry and biomarker thermal maturity to robustly capture earthquake temperature rise along the Punchbowl Fault, California. *Geochemistry, Geophysics, Geosystems*, 23(4), 1–20. https://doi.org/10.1029/2021GC010291
- Ault, A. K. (2020). Hematite fault rock thermochronometry and textures inform fault zone processes. *Journal of Structural Geology*, 133(November 2019), 104002. https://doi.org/10.1016/j.jsg.2020.104002
- Ault, A. K., Frenzel, M., Reiners, P. W., Woodcock, N. H., & Thomson, S. N. (2016). Record of paleofluid circulation in faults revealed by hematite (U-Th)/He and apatite fission-track dating: An example from Gower Peninsula fault fissures, Wales. *Lithosphere*, 8(4), 379–385. https://doi.org/10.1130/L522.1
- Ault, A. K., Jensen, J. L., McDermott, R. G., Shen, F.-A., & Van Devener, B. R. (2019). Nanoscale evidence for temperature-induced transient rheology and postseismic fault healing. *Geology*, 47(12), 1203–1207. https://doi.org/10.1130/G46317.1
- Ault, A. K., Reiners, P. W., Evans, J. P., & Thomson, S. N. (2015). Linking hematite (U-Th)/He dating with the microtextural record of seismicity in the Wasatch fault damage zone, Utah, USA. Geology, 43(9), 771–774. https://doi.org/10.1130/G36897.1
- Bähr, R., Lippolt, H. J., & Wernicke, R. S. (1994). Temperature-induced 4 He degassing of specularite and botryoidal hematite: A 4 He retentivity study. *Journal of Geophysical Research*, 99(B9), 17695–17707. https://doi.org/10.1029/94JB01055
- Banerjee, S. (1971). New grain size limits for palaeomagnetic stability in haematite. Nature Physical Science, 232(27), 15–16. https://doi.org/10.1038/physci232015a0
- Benson, L., Madole, R., Landis, G., & Gosse, J. (2005). New data for Late Pleistocene Pinedale alpine glaciation from southwestern Colorado. Quaternary Science Reviews, 24(1–2), 49–65. https://doi.org/10.1016/j.quascirev.2004.07.018
- Bryant, B., & Naeser, C. W. (1980). The significance of fission-track ages of apatite in relation to the tectonic history of the Front and Sawatch Ranges, Colorado. Geological Society of America Bulletin, 91(3), 156. https://doi.org/10.1130/0016-7606(1980)91<156:TSOFAO>2.0.CO;2

Acknowledgments
We thank Peter Reiners and Uttam

of Geosciences

JENSEN ET AL.

We thank Peter Reiners and Uttam Chowdhury (Univ. of Arizona) for science

assistance, respectively. We thank Ziaul Haque (UT Dallas) for the acquisition of new magnetic susceptibility measurements and Kara Williams (Colorado St. Univ.) for field sampling. We thank two anonymous reviewers for feedback that helped strengthen and clarify the manuscript. This work was supported by NSF grants PF-1144905, EAR-1419828, and EAR-1654628, all to Ault. Jensen acknowledges support from the Presidential Doctoral Research Fellowship of USU

and the Beryl O. and Tura H. Springer

Memorial Scholarship of the USU Dept.

discussions and (U-Th)/He analytical

5252027, 2023, 9, Downloaded from https

- Butler, R. F. (1992). Paleomagnetism Magnetic domains to geologic terranes. Blackwell Scientific Publications. Retrieved from https://www.researchgate.net/profile/Robert-Butler-11/publication/247098083_Paleomagnetism_Magnetic_Domains_to_Geologic_Terranes/links/544e62940cf26dda08900f0a/Paleomagnetism-Magnetic-Domains-to-Geologic-Terranes.pdf
- Calzolari, G., Ault, A. K., Hirth, G., & McDermott, R. G. (2020). Hematite (U-Th)/He thermochronometry detects asperity flash heating during laboratory earthquakes. *Geology*, 48(5), 514–518. https://doi.org/10.1130/G46965.1
- Cather, S. M., Chapin, C. E., & Kelley, S. A. (2012). Diachronous episodes of Cenozoic erosion in southwestern North America and their relationship to surface uplift, paleoclimate, paleodrainage, and paleoaltimetry. Geosphere, 8(6), 1177–1206. https://doi.org/10.1130/GES00801.1
- Chapin, C. E., & Kelley, S. A. (1997). The Rocky Mountain erosion surface in the Front Range of Colorado. In Colorado Front Range guide-book (p. 101). Rocky Mountain Association of Geologists. Retrieved from https://archives.datapages.com/data/rmag/geohistfrontrange1997/chapin b.html
- Cooperdock, E. H. G., Ketcham, R. A., & Stockli, D. F. (2019). Resolving the effects of 2-D versus 3-D grain measurements on apatite (U-Th) / He age data and reproducibility. *Geochronology*, 1(1), 17–41. https://doi.org/10.5194/gchron-1-17-2019
- Copeland, P., Currie, C. A., Lawton, T. F., & Murphy, M. A. (2017). Location, location, location: The variable lifespan of the laramide orogeny. Geology, 45(3), 223–226. https://doi.org/10.1130/G38810.1
- Creer, K. M. (1968). Palaeozoic Palaeomagnetism. Nature, 219(5151), 246-250. https://doi.org/10.1038/219246a0
- Danišík, M., Evans, N. J., Ramanaidou, E. R., McDonald, B. J., Mayers, C., & McInnes, B. I. A. (2013). (U–Th)/He chronology of the Robe River channel iron deposits, Hamersley Province, Western Australia. *Chemical Geology*, 354, 150–162. https://doi.org/10.1016/j. chemica.2013.06.012
- DiMonte, A. A., Ault, A. K., Hirth, G., & Bradbury, K. K. (2022). Hematite accommodated shallow, transient Pleistocene slow slip in the exhumed southern San Andreas fault system. California. USA. *Geology*, 50(12), 1443–1447, https://doi.org/10.1130/G50489.1
- Dodson, M. H. (1973). Closure temperature in cooling geochronological and petrological systems. Contributions to Mineralogy and Petrology, 40(3), 259–274. https://doi.org/10.1007/BF00373790
- Dodson, M. H., & McClelland-Brown, E. (1980). Magnetic blocking temperatures of single-domain grains during slow cooling. *Journal of Geophysical Research*, 85(B5), 2625. https://doi.org/10.1029/JB085iB05p02625
- Domeier, M., Van Der Voo, R., & Torsvik, T. H. (2012). Paleomagnetism and Pangea: The road to reconciliation. *Tectonophysics*, 514–517,
- 14–43. https://doi.org/10.1016/j.tecto.2011.10.021
 Dunlop, D. J., Özdemir, Ö., & Schmidt, P. W. (1997). Paleomagnetism and paleothermometry of the Sydney Basin 2. Origin of anomalously high
- unblocking temperatures. *Journal of Geophysical Research*, 102(12), 27285–27295. https://doi.org/10.1029/97jb02478
 Eaton, G. P. (2008). Epeirogeny in the southern Rocky Mountains region: Evidence and origin. *Geosphere*, 4(5), 764–784. https://doi.org/10.1130/
- Eaton, G. P. (2008). Epeirogeny in the southern Rocky Mountains region: Evidence and origin. *Geosphere*, 4(5), 764–784. https://doi.org/10.1130/GES00149.1
- Eckel, E. B. (1961). Minerals of Colorado: A 100-year record. https://doi.org/10.3133/b1114
- Elder, W. P., & Kirkland, J. I. (1994). Cretaceous paleogeography of the southern Western Interior region. In Mesozoic systems of the Rocky Mountain Region, USA (pp. 415–440).
- Elmore, R. D., Muxworthy, A. R., & Aldana, M. (2012). Remagnetization and chemical alteration of sedimentary rocks. *Geological Society Special Publications*, 371(1), 1–21. https://doi.org/10.1144/SP371.15
- Epis, R. C., & Chapin, C. E. (1974). Stratigraphic nomenclature of the Thirtynine Mile volcanic field, central Colorado (Issue 1395). US Government Printing Office
- Evenson, N. S., Reiners, P. W., Spencer, J. E., & Shuster, D. L. (2014). Hematite and Mn oxide (U-Th)/He dates from the Buckskin-Rawhide detachment system, Western Arizona: Gaining insights into hematite (U-Th)/He system. *American Journal of Science*, 314(10), 1373–1435. https://doi.org/10.2475/10.2014.01
- Farley, K. A. (2018). Helium diffusion parameters of hematite from a single-diffusion-domain crystal. *Geochimica et Cosmochimica Acta*, 231, 117–129. https://doi.org/10.1016/j.gca.2018.04.005
- Farley, K. A., & Flowers, R. M. (2012). (U-Th)/Ne and multidomain (U-Th)/He systematics of a hydrothermal hematite from eastern Grand Canyon. Earth and Planetary Science Letters, 359–360, 131–140. https://doi.org/10.1016/j.epsl.2012.10.010
- Flowers, R. M., Ketcham, R. A., Shuster, D. L., & Farley, K. A. (2009). Apatite (U-Th)/He thermochronometry using a radiation damage accumulation and annealing model. *Geochimica et Cosmochimica Acta*, 73(8), 2347–2365. https://doi.org/10.1016/j.gca.2009.01.015
- Flowers, R. M., MacDonald, F. A., Siddoway, C. S., & Havranek, R. (2020). Diachronous development of Great unconformities before neoprote-rozoic snowball Earth. *Proceedings of the National Academy of Sciences of the United States of America*, 117(19), 10172–10180. https://doi.org/10.1073/pnas.1913131117
- Frost, R. L., & Dickfos, M. J. (2007). Raman spectroscopy of halogen-containing carbonates. *Journal of Raman Spectroscopy*, 38(11), 1516–1522, https://doi.org/10.1002/jrs.1806
- Garcia, V. H., Reiners, P. W., Shuster, D. L., Idleman, B., & Zeitler, P. K. (2018). Thermochronology of sandstone-hosted secondary Fe- and Mn-oxides near Moab. Utah: Record of paleo-fluid flow along a fault. GSA Bulletin. 130(1–2), 93–113, https://doi.org/10.1130/B31627.1
- Geissman, J. W., & Harlan, S. S. (2002). Late Paleozoic remagnetization of Precambrian crystalline rocks along the Precambrian/Carboniferous nonconformity, Rocky Mountains: A relationship among deformation, remagnetization, and fluid migration. Earth and Planetary Science Letters, 203(3–4), 905–924. https://doi.org/10.1016/S0012-821X(02)00932-9
- Geissman, J. W., Jackson, M., Harlan, S. S., & Van Der Voo, R. (1991). Paleomagnetism of latest Cambrian-early Ordovician and latest Cretaceous-early tertiary rocks of the Florida Mountains, southwest New Mexico. *Journal of Geophysical Research*, 96(B4), 6053–6071. https://doi.org/10.1029/90JB02701
- Gordon, R. G., Cox, A., & O'Hare, S. (1984). Paleomagnetic Euler poles and the apparent polar wander and absolute motion of North America since the Carboniferous. *Tectonics*, 3(5), 499–537. https://doi.org/10.1029/TC003i005p00499
- Guenthner, W. R., Reiners, P. W., Ketcham, R. A., Nasdala, L., & Giester, G. (2013). Helium diffusion in natural zircon: Radiation damage, anisotropy, and the interpretation of zircon (U-TH)/He thermochronology. American Journal of Science, 313(3), 145–198. https://doi. org/10.2475/03.2013.01
- Havranek, R. E., & Flowers, R. M. (2022). Zircon (U-Th)/He data for the Colorado Front Range "fourteeners" and testing Cryogenian exhumation of sub-Great unconformity basement. *Chemical Geology*, 591(June 2021), 120702. https://doi.org/10.1016/j.chemgeo.2021.120702
- Hofmann, F., Treffkorn, J., & Farley, K. A. (2020). U-loss associated with laser-heating of hematite and goethite in vacuum during (U-Th)/He dating and prevention using high O, partial pressure. Chemical Geology, 532, 119350. https://doi.org/10.1016/j.chemgeo.2019.119350
- Huang, W., Lippert, P. C., Jackson, M. J., Dekkers, M. J., Zhang, Y., Li, J., et al. (2017). Remagnetization of the Paleogene Tibetan Himala-yan carbonate rocks in the Gamba area: Implications for reconstructing the lower plate in the India-Asia collision. *Journal of Geophysical Research: Solid Earth*, 122(2), 808–825. https://doi.org/10.1002/2016JB013662

JENSEN ET AL. 19 of 22

5252027, 2023, 9, Downloaded from https

onlinelibrary.wiley.com/doi/10.1029/2023GC010993,

- Huang, W., Niu, S., Dekkers, M. J., Lippert, P. C., Bilardello, D., Solheid, P., et al. (2023). Remagnetization under hydrothermal alteration of South Tibetan Paleocene lavas: Maghemitization, hematization, and grain size reduction of (Titano)magnetite. *Journal of Geophysical Research: Solid Earth*, 128(3), 1–26. https://doi.org/10.1029/2023JB026418
- Irving, E., & Parry, L. G. (1963). The magnetism of some Permian Rocks from New South Wales. *Geophysical Journal International*, 7(4), 395–411. https://doi.org/10.1111/j.1365-246X.1963.tb07084.x
- Jensen, J. L., Siddoway, C. S., Reiners, P. W., Ault, A. K., Thomson, S. N., & Steele-MacInnis, M. (2018). Single-crystal hematite (U-Th)/He dates and fluid inclusions document widespread Cryogenian sand injection in crystalline basement. Earth and Planetary Science Letters, 500, 145–155. https://doi.org/10.1016/j.epsl.2018.08.021
- Johnson, J., Flowers, R. M., Baird, G., & Mahan, K. (2017). "Inverted" zircon and apatite (U-Th)/He dates from the Front Range, Colorado: High damage zircon as a low temperture (<50°C) thermochronometer. Earth and Planetary Science Letters, 466, 80–90. https://doi.org/10.1016/j.epsl.2017.03.002</p>
- Kelley, S. A., & Blackwell, D. D. (2002). Subsurface temperatures in the southern Denver Basin, Colorado. Rocky Mountain Geology, 37(2), 215–227. https://doi.org/10.2113/gsrocky.37.2.215
- Kelley, S. A., & Chapin, C. E. (2004). Denudation history and internal structure of the Front Range and Wet Mountains, Colorado, based on apatite-fission-track thermochronology. New Mexico Bureau of Geology & Mineral Resources Bulletin, 160, 41–77.
- Kellogg, K. S., Bryant, B., & Reed, J. C. (2004). The Colorado Front Range—Anatomy of a Laramide uplift. GSA Field Guide 5: Field Trips in the Southern Rocky Mountains, USA, 5, 89–108. https://doi.org/10.1130/0-8137-0005-1
- Kellogg, K. S., Shroba, R. R., Bryant, B., & Premo, W. R. (2008). Geologic map of the Denver West 30' x 60' quadrangle, north-central Colorado. https://doi.org/10.3133/sim3000
- Ketcham, R. A. (2005). Forward and inverse modeling of low-temperature thermochronometry data. Reviews in Mineralogy and Geochemistry, 58(1), 275–314. https://doi.org/10.2138/rmg.2005.58.11
- Ketcham, R. A., Carter, A., Donelick, R. A., Barbarand, J., & Hurford, A. J. (2007). Improved modeling of fission-track annealing in apatite. American Mineralogist, 92(5–6), 799–810. https://doi.org/10.2138/am.2007.2281
- Ketcham, R. A., Gautheron, C., & Tassan-Got, L. (2011). Accounting for long alpha-particle stopping distances in (U-Th-Sm)/He geochronology: Refinement of the baseline case. Geochimica et Cosmochimica Acta, 75(24), 7779–7791. https://doi.org/10.1016/j.gca.2011.10.011
- Kletetschka, G., & Wasilewski, P. J. (2002). Grain size limit for SD hematite. *Physics of the Earth and Planetary Interiors*, 129(1–2), 173–179. https://doi.org/10.1016/S0031-9201(01)00271-0
- Kluth, C. F., & Coney, P. J. (1981). Plate tectonics of the Ancestral Rocky Mountains. Geology, 9(1), 10–15. https://doi.org/10.1130/0091-7613(1981)9<10
- Larson, E. E., Walker, T. R., Patterson, P. E., Hoblitt, R. P., & Rosenbaum, J. G. (1982). Paleomagnetism of the Moenkopi formation, Colorado Plateau: Basis for long-term model of acquisition of chemical remanent magnetism in red beds. *Journal of Geophysical Research*, 87(B2),
- 1081–1106. https://doi.org/10.1029/JB087iB02p01081

 Leary, R. J., Umhoefer, P., Smith, M. E., & Riggs, N. (2017). A three-sided orogen: A new tectonic model for Ancestral Rocky Mountain uplift and basin development. *Geology*, 45(8), 735–738. https://doi.org/10.1130/G39041.1
- Li, X. C., Yang, K. F., Spandler, C., Fan, H. R., Zhou, M. F., Hao, J. L., & Yang, Y. H. (2021). The effect of fluid-aided modification on the Sm-Nd and Th-Pb geochronology of monazite and bastnäsite: Implication for resolving complex isotopic age data in REE ore systems. *Geochimica et Cosmochimica Acta*, 300, 1–24. https://doi.org/10.1016/j.gca.2021.02.028
- Lide, D. R. (1997). Abundance of elements in the Earth's crust and sea. In CRC handbook of physics and chemistry (78th ed., p. 14).
- Lippolt, H. J., & Weigel, E. (1988). 4He diffusion in 40Ar-retentive minerals. Geochimica et Cosmochimica Acta, 52(6), 1449–1458. https://doi.org/10.1016/0016-7037(88)90215-3
- Madole, R. F., Bradley, W. C., Loewenherz, D. S., Ritter, D. F., Rutter, N. W., & Thorn, C. E. (1987). Rocky Mountains. In Geomorphic systems of North America (pp. 211–257). Geological Society of America. https://doi.org/10.1130/DNAG-CENT-v2.211
- McDermott, R. G., Ault, A. K., & Caine, J. S. (2021). Dating fault damage along the eastern Denali fault zone with hematite (U-Th)/He thermochronometry. Earth and Planetary Science Letters, 563, 116872. https://doi.org/10.1016/j.epsl.2021.116872
- McDermott, R. G., Ault, A. K., Evans, J. P., & Reiners, P. W. (2017). Thermochronometric and textural evidence for seismicity via asperity flash heating on exhumed hematite fault mirrors, Wasatch fault zone, UT, USA. *Earth and Planetary Science Letters*, 471, 85–93. https://doi.org/10.1016/j.epsl.2017.04.020
- McDermott, R. G., Ault, A. K., Wetzel, K. F., Evans, J. P., & Shen, F. (2023). Microscale spatial variations in coseismic temperature rise on hematite fault mirrors in the Wasatch fault damage zone. *Journal of Geophysical Research: Solid Earth*, 128(3), 1–20. https://doi.org/10.1029/2022jb025069
- Meert, J. G. (2001). Growing Gondwana and Rethinking Rodinia: A paleomagnetic perspective. Gondwana Research, 4(3), 279–288. https://doi.org/10.1016/S1342-937X(05)70329-4
- Monteiro, H. S., Vasconcelos, P. M., Farley, K. A., Mello, C. L., & Conceição, F. T. (2022). Long-term vegetation-induced goethite and hematite dissolution-reprecipitation along the Brazilian Atlantic margin. *Palaeogeography, Palaeoclimatology, Palaeoecology*, 601(November 2021), 601. https://doi.org/10.1016/j.palaeo.2022.111137
- Moser, A. C., Evans, J. P., Ault, A. K., Janecke, S. U., & Bradbury, K. K. (2017). (U-Th)/He thermochronometry reveals Pleistocene punctuated deformation and synkinematic hematite mineralization in the Mecca Hills, southernmost San Andreas Fault zone. Earth and Planetary Science Letters, 476, 87–99. https://doi.org/10.1016/j.epsl.2017.07.039
- Murray, K. E., Orme, D. A., & Reiners, P. W. (2014). Effects of U-Th-rich grain boundary phases on apatite helium ages. *Chemical Geology*, 390, 135–151. https://doi.org/10.1016/j.chemgeo.2014.09.023
- Naeser, C. W., Bryant, B., Kunk, M. J., Kellogg, K., Donelick, R. A., & Perry, W. J. (2002). Tertiary cooling and tectonic history of the White River uplift, Gore Range, and western Front Range, central Colorado: Evidence from fission-track and 39 Ar/40 Ar ages (Vol. 366, pp. 31–53). Geological Society of America Special Paper. https://doi.org/10.1130/0-8137-2366-3.31
- Odlum, M. L., Ault, A. K., Channer, M. A., & Calzolari, G. (2022). Seismicity recorded in hematite fault mirrors in the Rio Grande rift. Geosphere, 18(1), 241–260. https://doi.org/10.1130/GES02426.1
- Opdyke, N. D. (1995). Magnetostratigraphy of Permo-Carboniferous time. In *Geochronology, time scales and global stratigraphic correlation*. SEPM Society for Sedimentary Geology. https://doi.org/10.2110/pec.95.04.0041
- Özdemir, Ö., & Dunlop, D. J. (2014). Hysteresis and coercivity of hematite. *Journal of Geophysical Research: Solid Earth*, 119(4), 2582–2594. https://doi.org/10.1002/2013JB010739
- Pearson, R. C., & Johnson, G. (1980). Mineral resources of the Indian Peaks study area, Boulder and Grand counties, Colorado, with a section on interpretation of aeromagnetic data. https://doi.org/10.3133/b1463

JENSEN ET AL. 20 of 22

5252027, 2023, 9, Downloaded from

wiley.com/doi/10.1029/2023GC010993,

of use; OA articles are governed by the applicable Creative Commons Licens

- Peterman, Z. E., Hedge, C. E., & Braddock, W. A. (1968). Age of Precambrian events in the Northeastern Front Range, Colorado. *Journal of Geophysical Research*, 73(6), 2277–2296. https://doi.org/10.1029/jb073i006p02277
- Pivarunas, A. F., & Meert, J. G. (2019). Protracted magmatism and magnetization around the McClure Mountain alkaline igneous complex. Lithosphere, 11(5), 590–602. https://doi.org/10.1130/L1062.1
- Preeden, U., Mertanen, S., Elminen, T., & Plado, J. (2009). Secondary magnetizations in shear and fault zones in southern Finland. *Tectonophysics*, 479(3–4), 203–213. https://doi.org/10.1016/j.tecto.2009.08.011
- Premo, W. R., & Fanning, C. M. (2000). SHRIMP U-Pb zircon ages for Big Creek gneiss, Wyoming and Boulder Creek batholith, Colorado: Implications for timing of Paleoproterozoic accretion of the northern Colorado province. *Rocky Mountain Geology*, 35(1), 31–50. https://doi.org/10.2113/35.1.31
- Pullaiah, G., Irving, E., Buchan, K. L., & Dunlop, D. J. (1975). Magnetization changes caused by burial and uplift. Earth and Planetary Science Letters, 28(2), 133–143. https://doi.org/10.1016/0012-821X(75)90221-6
- Raschke, M. B., Stern, C. R., Anderson, E. J. D., Skewes, M. A., Farmer, G. L., Allaz, J. M., & Persson, P. M. (2021). Bulk composition of a zoned rare-earth minerals-bearing pegmatite in the Pikes Peak granite batholith near Wellington Lake, central Colorado, U.S.A. Rocky Mountain Geology, 56(1), 1–18. https://doi.org/10.24872/rmgjournal.56.1.1
- Reed, J. C., Wheeler, J. O., & Tucholke, B. E. (2004). Geologic map of North America: Decade of North American geology continental scale map 001. Retrieved from https://www.usgs.gov/media/images/geologic-map-north-america
- Reiners, P. W., Chan, M. A., & Evenson, N. S. (2014). (U-Th)/He geochronology and chemical compositions of diagenetic cement, concretions, and fracture-filling oxide minerals in Mesozoic sandstones of the Colorado Plateau. Geological Society of America Bulletin, 126(9–10), 1363–1383. https://doi.org/10.1130/B30983.1
- Ricketts, J. W., Roiz, J., Karlstrom, K. E., Heizler, M. T., Guenthner, W. R., & Timmons, J. M. (2021). Tectonic controls on basement exhumation in the southern Rocky Mountains (United States): The power of combined zircon (U-Th)/He and K-feldspar 40Ar/39Ar thermochronology. Geology, 49(10), 1187–1192. https://doi.org/10.1130/G49141.1
- Roy, J. L., & Park, J. K. (1972). Red beds: DRM or CRM? Earth and Planetary Science Letters, 17(1), 211-216. https://doi.org/10.1016/0012-821X(72)90279-8
- Schneider, C. A., Rasband, W. S., & Eliceiri, K. W. (2012). NIH Image to ImageJ: 25 years of image analysis. *Nature Methods*, 9(7), 671–675. https://doi.org/10.1038/nmeth.2089
- Schütz, F., Winterleitner, G., & Huenges, E. (2018). Geothermal exploration in a sedimentary basin: New continuous temperature data and physical rock properties from northern Oman. *Geothermal Energy*, 6(1), 5. https://doi.org/10.1186/s40517-018-0091-6
- Scott, G. R. (1972). Geologic map of the Morrison Quadrangle, Jefferson County, Colorado. https://doi.org/10.3133/i790A
- Shuster, D. L., & Farley, K. A. (2005). Diffusion kinetics of proton-induced ²¹Ne, ³He, and ⁴He in quartz. *Geochimica et Cosmochimica Acta*, 69(9), 2349–2359. https://doi.org/10.1016/j.gca.2004.11.002
- Shuster, D. L., Flowers, R. M., & Farley, K. A. (2006). The influence of natural radiation damage on helium diffusion kinetics in apatite. *Earth and Planetary Science Letters*, 249(3–4), 148–161. https://doi.org/10.1016/j.epsl.2006.07.028
- Spiegel, C., Kohn, B., Belton, D., Berner, Z., & Gleadow, A. (2009). Apatite (U-Th-Sm)/He thermochronology of rapidly cooled samples: The effect of He implantation. Earth and Planetary Science Letters, 285(1-2), 105-114. https://doi.org/10.1016/j.epsl.2009.05.045
- Strutt, R. J. (1910). Measurements of the rate at which Helium is produced in Thorianite and Pitchblende, with a minimum estimate of their antiquity. Proceedings of the Royal Society of London Series A: Containing Papers of a Mathematical and Physical Character, 84(571), 379–388. https://doi.org/10.1098/rspa.1910.0083
- Sweet, D. E., Carsrud, C. R., & Watters, A. J. (2015). Proposing an entirely Pennsylvanian Age for the Fountain Formation through new lithostratigraphic correlation along the Front Range. *Mountain Geologist*, 52(2), 43–70. https://doi.org/10.31582/rmag.mg.52.2.43
- Torsvik, T. H. (2005). Palaeomagnetism. In *Encyclopedia of geology* (Vol. 90, pp. 147–156). Elsevier. https://doi.org/10.1016/B0-12-369396-9/00106-4
- Tourtelot, H. A. (1962). Preliminary investigation of the geologic setting and chemical composition of the Pierre Shale, Great Plains region. https://doi.org/10.3133/pp390
- Tweto, O. (1975). Laramide (Late Cretaceous-Early Tertiary) Orogeny in the Southern Rocky Mountains. In B. F. Curtis (Ed.), Cenozoic history of the southern Rocky mountains (pp. 1–44). Geological Society of America. https://doi.org/10.1130/MEM144-p1
- Tweto, O. (1979). Geologic map of Colorado. Retrieved from https://coloradogeologicalsurvey.org/publications/tweto-geologic-map-colorado-1979
 Van der Voo, R., & French, R. B. (1977). Paleomagnetism of the Late Ordovician Juniata formation and the remagnetization hypothesis. *Journal of Geophysical Research*, 82(36), 5796–5802. https://doi.org/10.1029/jb082i036p05796
- Vasconcelos, P. M., Heim, J. A., Farley, K. A., Monteiro, H., & Waltenberg, K. (2013). 40Ar/39Ar and (U-Th)/He 4He/3He geochronology of landscape evolution and channel iron deposit genesis at Lynn Peak, Western Australia. Geochimica et Cosmochimica Acta, 117, 283–312. https://doi.org/10.1016/j.gca.2013.03.037
- Wawrzyniec, T. F., Ault, A. K., Geissman, J. W., Erslev, E. A., & Fankhauser, S. D. (2007). Paleomagnetic dating of fault slip in the Southern Rocky Mountains, USA, and its importance to an integrated Laramide foreland strain field. *Geosphere*, 3(1), 16–25. https://doi.org/10.1130/GES00066.1
- Weimer, R. J., & Sonnenberg, S. A. (1996). Guide to the petroleum geology and Laramide orogeny, Denver Basin and Front Range, Colorado. Colorado Geological Survey, Department of Natural Resources.
- Wernicke, R. S., & Lippolt, H. J. (1993). Botryoidal hematite from the Schwarzwald (Germany): Heterogeneous uranium distributions and their bearing on the helium dating method. Earth and Planetary Science Letters, 114(2–3), 287–300. https://doi.org/10.1016/0012-821X(93)90031-4
- Whitmeyer, S., & Karlstrom, K. (2007). Tectonic model for the Proterozoic growth of North America. Geosphere, 3(4), 220. https://doi.org/10.1130/GES00055.1
- Wu, L. Y., Stuart, F. M., Di Nicola, L., Heizler, M., Benvenuti, M., & Hu, R. Z. (2018). Multi-aliquot method for determining (U + Th)/He ages of hydrothermal hematite: Returning to Elba. Chemical Geology, 504(November), 1–7. https://doi.org/10.1016/j.chemgeo.2018.11.005
- Zhang, S., Li, Z. X., Evans, D. A. D., Wu, H., Li, H., & Dong, J. (2012). Pre-Rodinia supercontinent Nuna shaping up: A global synthesis with new paleomagnetic results from North China. Earth and Planetary Science Letters, 353–354, 145–155. https://doi.org/10.1016/j.epsl.2012.07.034

JENSEN ET AL. 21 of 22

15252027, 2023, 9, Downloaded from https://agupubs

.onlinelibrary.wiley.com/doi/10.1029/2023GC010993, Wiley Online Library on [16/09/2023]. See the Terms and Conditions (https://onlinelibrary.wiley.com/terms-and-conditions) on Wiley Online Library for rules of use; OA articles are governed by the applicable Creative Commons License

References From the Supporting Information

- Blackburn, T. J., Stockli, D. F., & Walker, J. D. (2007). Magnetite (U-Th)/He dating and its application to the geochronology of intermediate to mafic volcanic rocks. Earth and Planetary Science Letters, 259(3–4), 360–371. https://doi.org/10.1016/j.epsl.2007.04.044
- Farley, K. A. (2002). (U-Th)/He dating: Techniques, calibrations, and applications. Reviews in Mineralogy and Geochemistry, 47(1), 819–844. https://doi.org/10.2138/rmg.2002.47.18
- Kuiper, K. F., Deino, A., Hilgen, F. J., Krijgsman, W., Renne, P. R., & Wijbrans, J. R. (2008). Synchronizing Rock Clocks of Earth History. Science, 320(5875), 500–504. https://doi.org/10.1126/science.1154339
- McDowell, F. W., McIntosh, W. C., & Farley, K. A. (2005). A precise 40Ar-39Ar reference agefor the Durango apatite (U-Th)/He and fission-track dating standard. *Chemical Geology*, 214(3-4), 249-263. https://doi.org/10.1016/j.chemgeo.2004.10.002
- Wolf, R. A., Farley, K. A., & Kass, D. M. (1998). Modeling of the temperature sensitivity of theapatite (U-Th)/He thermochronometer. Chemical Geology, 148(1–2), 105–114. https://doi.org/10.1016/S0009-2541(98)00024-2

JENSEN ET AL. 22 of 22